ELSEVIER

Journal of South American Earth Sciences 18 (2005) 125–145

Journal of
South American
Earth Sciences

www.elsevier.com/locate/jsames

The upper mantle beneath Patagonia, Argentina, documented by xenoliths from alkali basalts

E.A. Bjerg[a,*], T. Ntaflos[b], G. Kurat[b], G. Dobosi[c], C.H. Labudía[a]

[a]*Departamento de Geología, CONICET—Universidad Nacional del Sur, San Juan 670, B8000ICN Bahía Blanca, Argentina*
[b]*Department of Geological Sciences, University of Vienna, Althanstrasse 14, A-1090 Vienna, Austria*
[c]*Hungarian Academy of Sciences, Laboratory for Geochemical Research, Budaörsiút 45, H-1112 Budapest, Hungary*

Received 1 March 2003; accepted 1 September 2004

Abstract

Mantle xenoliths in alkali basaltic lavas (with ocean-island basalt chemical signatures) and cinder cones occur in several areas of Patagonia. A representative suite of mantle xenoliths was collected in the region between latitudes 40° and 52°S and longitudes 67° and 71°W in the Río Negro, Chubut, and Santa Cruz provinces, Argentina. Mantle xenoliths in Patagonia display distinguishing peculiarities compared with those of other worldwide occurrences. The lithospheric mantle beneath Patagonia, as inferred from chemical variation diagrams, has experienced only minor melt extractions in the garnet peridotite field and more extensive melt extractions in the spinel lherzolite field. Variably intensive cryptic and modal metasomatism affected the lithospheric mantle in this region. Textural evidence shows that the mantle is moderately to strongly tectonized and recrystallized on both the local and the regional scale, with an overall predominance of deformed textural types. Mineral equilibrium indicates a strongly elevated geotherm similar to the southeast Australia and oceanic geotherms, which is not normal for a continental intraplate tectonic setting. Therefore, the properties of the Patagonian samples are probably related to the presence of rising mantle plume(s) in an extensional tectonic setting.

Keywords: Alkali basalts; Garnet; Metasomatism; Patagonia; Upper mantle; Xenoliths

Resumen

Asociados a lavas basálticas alcalinas (con signatura química OIB) y conos de cineritas se han reconocidos xenolitos mantélicos en varias areas de Patagonia. Un conjunto representativo de xenolitos del manto fueron recolectados en la región comprendida entre las latitudes 40° a 52°S y las longitudes 67° a 71°W en las provincias de Río Negro, Chubut, y Santa Cruz, República Argentina. Los xenolitos mantélicos de Patagonia presentan algunas características peculiares en comparación con las correspondientes a los hallados en otras partes del mundo. El manto litósferico que la subyace ha experimentado solo extracciones menores de fundidos en el campo de estabilidad de las peridotitas granatíferas y mayores en el correspondiente a las lherzolitas espinélicas, tal como lo indican los diagramas de variación química. El manto litosférico de esta región ha sido afectado en forma variable por metasomatismo modal y críptico. Las evidencias texturales indican que el manto esta tectonizado y recristalzado en grados que varían de moderado a intenso, tanto a escala local como regional, con un claro predominio de los tipos texturales deformados. Los equilibrios minerales indican la presencia de una geoterma extremadamente alta, similar a la geoterma de South East Australia y las geotermas oceánicas. Esto no es normal para un ambiente tectónico de intraplaca. Por ello sugerimos que las características evidenciadas por los xenolitos de Patagonia son muy probablemente el resultado de la presencia de pluma(s) de manto ascendente(s), en un ambiente tectónico extensional.

1. Introduction

The geologic evolution of South America remains a matter of discussion because the available geologic

* Corresponding author. Fax: +54 291 4595148.
E-mail address: ebjerg@criba.edu.ar (E.A. Bjerg).

0895-9811/$ - see front matter © 2004 Published by Elsevier Ltd.
doi:10.1016/j.jsames.2004.09.002

information is far from complete. Most xenolith localities in South America have been discovered in the past 25 years, and Patagonia in particular offers an outstanding opportunity to gather information about the nature of the subcontinental lithospheric mantle at this latitude.

Upper mantle xenoliths in Patagonian basalts in Argentina have been reported by Villar (1975), Gelós and Hayase (1979), Skewes and Stern (1979), Gelós and Labudía (1981), Labudía et al. (1984, 1990), Stern et al. (1986, 1999), Stern (1989), Bjerg et al. (1991, 1994), and Varela et al. (1995). In recent years, Stern et al. (1990), Barbieri (1998), Kilian et al. (1998a,b, 2002), Ntaflos et al. (1998, 1999, 2000, 2001), Barbieri et al. (1999), Laurora et al. (1999, 2001), Dobosi et al. (1999), Bjerg et al. (1999a,b, 2000, 2002), Vannucci et al. (2002), Mazzucchelli et al. (2002), and Rivalenti et al. (2002) have contributed to a better understanding of the petrology and geochemistry of the upper mantle, the metasomatic processes that took place (and still take place) in the upper mantle, and the origin of the fluids responsible for metasomatism. On the basis of a study of xenoliths from northern Patagonia, Varela et al. (1997) have shown that metasomatism and tectonization were significant processes that affected xenoliths, many of which originated at a depth close to the garnet stability field.

We provide the results of our studies of upper mantle xenoliths from Pliocene–Pleistocene alkali basalts in an area between latitudes 40°–52°S and longitudes 67°–71°W. These data, together with those reported previously, provide some insight into the upper mantle underneath Patagonia and its geochemical evolution in recent geological times.

2. Geological setting

The Andean Cordillera represents the western continental margin of the South American plate whose geologic evolution is related to the subduction of the Nazca and Antarctic plates below the South American plate. South of 39°S, the Andean Cordillera can be divided in two major regions (Fig. 1). The southern volcanic zone (SVZ) extends to 46°S and is followed by a gap in volcanic activity due to the Chile Triple Junction (Ramos, 1999). The gap separates the SVZ from the Austral volcanic zone, which extends from 49° to 53°S (Stern and Kilian, 1996).

In Patagonia, Pliocene and Quaternary alkalic lavas carrying ultramafic xenoliths erupted east of the stratovolcanos of the actual orogenic arc and occupy a backarc tectonic environment. These lavas were classified as cratonic by Stern et al. (1990) and have geochemical characteristics similar to intraplate oceanic island basalts.

The regional geology of Patagonia, which is beyond the scope of this article, has been reported by several authors; for a synthesis of the regional geology, see Caminos (1999) and references therein.

3. Sampling localities

A representative suite of peridotitic xenoliths was collected in several localities of the Río Negro, Chubut, and Santa Cruz provinces (Fig. 1). In Río Negro, samples were collected along a 190 km regional profile extending between 41°01′S–70°15′W and 40°30′S–68°03′W at the following localities: Comallo, Laguna Fría, Traful, and Prahuaniyeu. Along this profile, xenoliths occur in late Pliocene–Early Pleistocene alkali lava flows, necks, and cinder cones, which postdate Miocene meseta lava flows. At Comallo, mostly small (2–4 cm), deep red, oxidized xenoliths occur in a cinder cone, whereas unaltered websterites, harzburgites, and lherzolites are present in the lava flow, which occurs on top of the cinder cone. At the Traful basaltic neck and Laguna Fría lava flows, unaltered harzburgites and lherzolites reach 30 cm in diameter. Prahuaniyeu is the farthest northern locality in Patagonia where garnet xenoliths have been discovered. The dominant types are spinel peridotites, as well as garnet peridotites, transitional spinel garnet peridotites, and few pyroxenites. At this locality, xenoliths occur in both a cinder cone and a small lava flow.

In Chubut (Ch) province, samples were collected in the area of Paso de Indios (43°49′S–69°02′W). Websterites, harzburgites, lherzolites, and dunites, up to 10 cm in size, are hosted by Oligocene alkali basalt necks and lava flows.

In Santa Cruz, mantle xenoliths were collected at the Gobernador Gregores (DUB), Tres Lagos (TL), and Pali Aike (PA) localities. Some of the largest Patagonia xenoliths (up to 40 cm) occur at Gobernador Gregores (48°34′S–70°11′W) in a deeply eroded cinder cone (2.5 km diameter). The collected samples comprise spinel harzburgites, lherzolites, and wehrlites. Amphibole, secondary calcite, and phlogopite-bearing wehrlites, lherzolites, and harzburgites contain glassy patches up to 1 cm in diameter. Xenoliths from Gobernador Gregores, compared with xenoliths from the other localities, are unusually coarse grained.

At Tres Lagos (49°11′S–71°20′W), the xenolith sizes range between 4 and 20 cm, and they occur in a cinder cone. Most show deep red colors due to oxidation. Unaltered xenoliths are found associated with basalt dikes (∼40–50 cm wide), which cut the cinder cone, and small lava flows related to this cinder cone.

At Pali Aike, a large volcanic field extending along the southernmost E–W border between Argentina and Chile (51°49′S–69°41′W), xenoliths between 2 and 8 cm occur in three tephra levels. Harzburgites are dominant, followed by spinel lherzolites, wehrlites, orthopyroxenites, and garnet-bearing lherzolites.

4. Analytical methods

Electron microprobe analyses of major minerals were carried out with a Cameca SX 100 electron microprobe

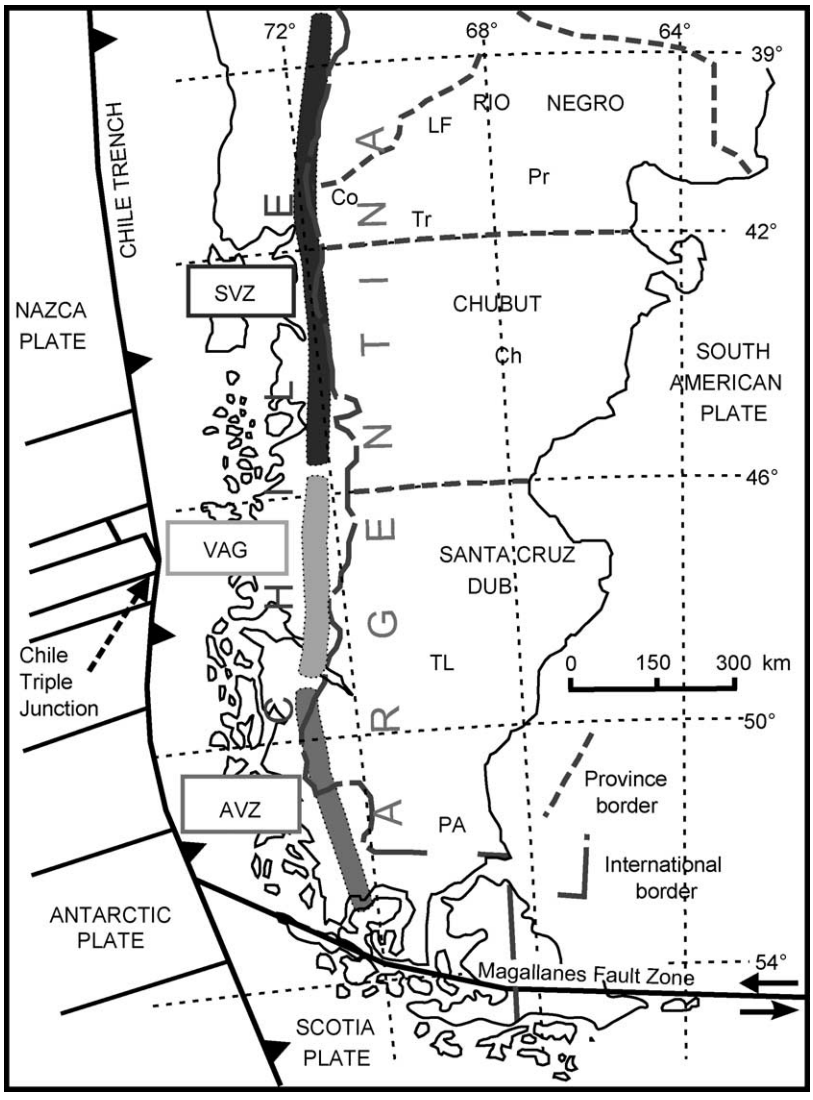

Fig. 1. Localities in Patagonia with ultramafic xenolith occurrences. Co, Comallo; Ch, Paso de Indios; DUB, Gobernador Gregores; LF, Laguna Fría; PA, Pali Aike; Pr, Prahuaniyeu; TL, Tres Lagos; Tr, Traful.

(University of Vienna). All analyses were made against mineral standards with wavelength-dispersive spectro meters; acceleration voltage and beam current were 15 kV and 20 nA, respectively, and standard correction procedures were applied.

To eliminate the effect of secondary X-ray fluorescence (XRF) between coexisting clinopyroxene and olivine, olivines from several samples were separated for microprobe analyses. For Ca calibration, wollastonite was used as primary standard with the San Carlos olivine analyzed previously by INAA as secondary standard. Major and trace element analyses were carried out with XRF techniques (Philips 2400). Major elements were measured on fused disks and trace elements on pressed pallets. Ta, Th, U, Hf, Ir, Au, and rare earth elements (REE) were determined by INAA using the method described by Kruse and Spettel (1979).

Abundances of approximately 30 trace elements were determined in situ in selected minerals and glasses by laser ablation inductively coupled plasma mass spectrometry (LA-ICP-MS) (Department of Earth Sciences, Memorial University of Newfoundland, St John's, Newfoundland). The LA system used in this study is described in detail by Jackson et al. (1992), Jenner et al. (1994) and Horn et al. (1997). The measurements were carried out with a Fisons VG PQ2+ ICP-MS instrument using time-resolved analysis data acquisition software operating in fast, peak-jumping mode. Spiked silicate glass NIST 612 was used for calibration, and BCR-2 glass was used as secondary standard. Calcium was used as an internal standard to correct the ablation yield differences among the individual analyses. Data were reduced using the LAMTRACE© spreadsheet software written by S. Jackson.

5. Xenolith petrography

The xenolith collection from Patagonia comprises spinel harzburgites, garnet harzburgites, garnet spinel harzburgites, spinel lherzolites, spinel websterites, and minor amounts of wehrlites, dunites, and pyroxenites. A few xenoliths are composite made up of pyroxene-rich veins (olivine websterites and websterites) that crosscut lherzolites and dunites; the contact with the host lavas generally is sharp. In Tables 1A and B, we summarize the relative proportions of rock types in the studied localities, the relationship between rock types and dominant textures, and indications of garnet, pyroxene-Cr spinel symplectites, and metasomatic phases (hydrous minerals and/or glass veins and pockets).

The dominant texture, after Mercier and Nicolas (1975), is porphyroclastic (PO, Fig. 2a), followed by equigranular—both tabular (ET, Fig. 2b) and mosaic (EM, Fig. 2c)—and protogranular (PR) and transitional types are also present.

Coarse-grained, anhedral olivines are generally strained and kinked; very rarely, they include small, rounded, sulfide and pyroxene inclusions. The small olivine neoblasts in the xenoliths with porphyroclastic, equigranular, and transitional textures are strain free and show straight grain boundaries. Both orthopyroxenes and clinopyroxenes are strained but to a lesser extent than olivines, as is clearly visible because when clinopyroxene carries orthopyroxene exsolutions and vice versa, the exsolutions are slightly bent (Fig. 2d). Clinopyroxene grains are smaller than other silicate phases and generally interstitial. Both orthopyroxene and clinopyroxene carry exsolutions of spinel in the form of thin rods.

Brown spinels are present in all textural types and form anhedral, small interstitial, and vermicular grains in orthopyroxene-clinopyroxene-spinel symplectites (Fig. 2e). Sulfides are present as very thin veinlets (10 μm wide) along-grain boundaries, as droplets in silicates, and in fractures in silicates and oxides. Glass and/or hydrous phases (amphibole, phlogopite) are present in upper mantle xenoliths from both northern and southern Patagonia localities: Comallo (amphibole, Fig. 2f, Table 2), Prahuaniyeu (glass veins), Gobernador Gregores (glass veins, amphibole, and phlogopite, Table 2), Tres Lagos (glass veins), and Pali Aike (glass veins, phlogopite).

Amphibole- and phlogopite-bearing wehrlites from Gobernador Gregores (Table 2) are of particular interest because they contain melt pockets up to 1 cm in diameter (Ntaflos et al., 1998, 1999; Laurora et al., 2001) that consist of euhedral clinopyroxene, spinel, olivine, and glass ± calcite (Fig. 2g). Green chromian diopside has a spongy envelope that consists of intergrowths of pale-green clinopyroxene (cpx) and a brownish melt. Fine-grained spinel (sp) appears only as an inclusion in olivine (ol) and forms trails along the boundary with melt pockets. Disseminated dark phlogopite plates (Fig. 2h) and pargasitic amphiboles (amph) are crosscut by veins of a brownish melt. The melt pockets are normally in contact with olivine

Table 1A
Frequency in percentage of mantle xenolith rock types in the sampled locations in Patagonia

Locality	Websterite	Harzburgite	Lherzolite	Wehrlite	Dunite	Pyroxenite	Symplectites/garnet	Amphibole/phlogopite	Glass veinlets/glass patches
Comallo	17	50	33	n.p.	n.p.	n.p.	No/No	Yes/No	Yes/No
Laguna Fría	n.p.	82	18	n.p.	n.p.	n.p.	Yes/No	No/No	Yes/No
Traful	n.p.	58	33	n.p.	n.p.	n.p.	No/No	No/No	No/No
Prahuaniyeu	4	35	61	n.p.	n.p.	n.p.	Yes/Yes	No/Yes	Yes/No
Chubut	25	25	25	n.p.	25	n.p.	No/No	No/No	No/No
G. Gregores	n.p.	59	36	5	n.p.	n.p.	No/No	Yes/Yes	Yes/Yes
Tres Lagos	4	78	13	n.p.	4	n.p.	No/No	No/No	Yes/No
Pali Aike	n.p.	77	9	5	n.p.	9	No/Yes	No/Yes	No/No

Table 1B
Frequency in percentage of mantle xenolith textural types in the sampled locations in Patagonia

Locality	PR	PR to PO	PO	PO to EM	PO to ET	EM	ET	EM to ET
Comallo	n.p.	n.p.	n.p.	n.p.	n.p.	58	33	8
Laguna Fría	n.p.	n.p.	56	22	n.p.	22	n.p.	n.p.
Traful	n.p.	n.p.	20	20	20	40	n.p.	n.p.
Prahuaniyeu	n.p.	17	83	n.p.	n.p.	n.p.	n.p.	n.p.
Chubut	25	25	25	n.p.	n.p.	25	n.p.	n.p.
G. Gregores	10	40	10	n.p.	n.p.	40	n.p.	n.p.
Tres Lagos	10	n.p.	33	24	n.p.	33	n.p.	n.p.
Pali Aike	n.p.	30	25	5	10	20	5	5
Total	4	10	33	12	5	30	5	2

Notes. n.p., not present; PR, protogranular; PO, porphyroclastic; EM, equigranular mosaic; ET, equigranular tabular; to, transitional.

and orthopyroxene and, unlike some veinlets, do not show any continuity with the groundmass of the host basalt.

Garnet peridotites, garnet-spinel peridotites and garnet-bearing spinel clinopyroxenites are present at Prahuaniyeu in northern Patagonia (Ntaflos et al., 2001, 2002) and Pali Aike in the south (Stern et al., 1986). At both localities, garnet is typically surrounded by kelyphytic rims of variable thickness composed of a fine-grained intergrowth of orthopyroxene, clinopyroxene, and spinel (Fig. 2i). Garnet lherzolites from the Pali Aike volcanic field also carry glass veinlets and phlogopite. A detailed petrographic description of the xenoliths in each studied locality is included in Appendix 1.

6. Bulk-rock geochemistry

6.1. Major and minor elements

Patagonian peridotites display a wide range of major and minor element abundances (Table 3, Fig. 3a–e). The MgO

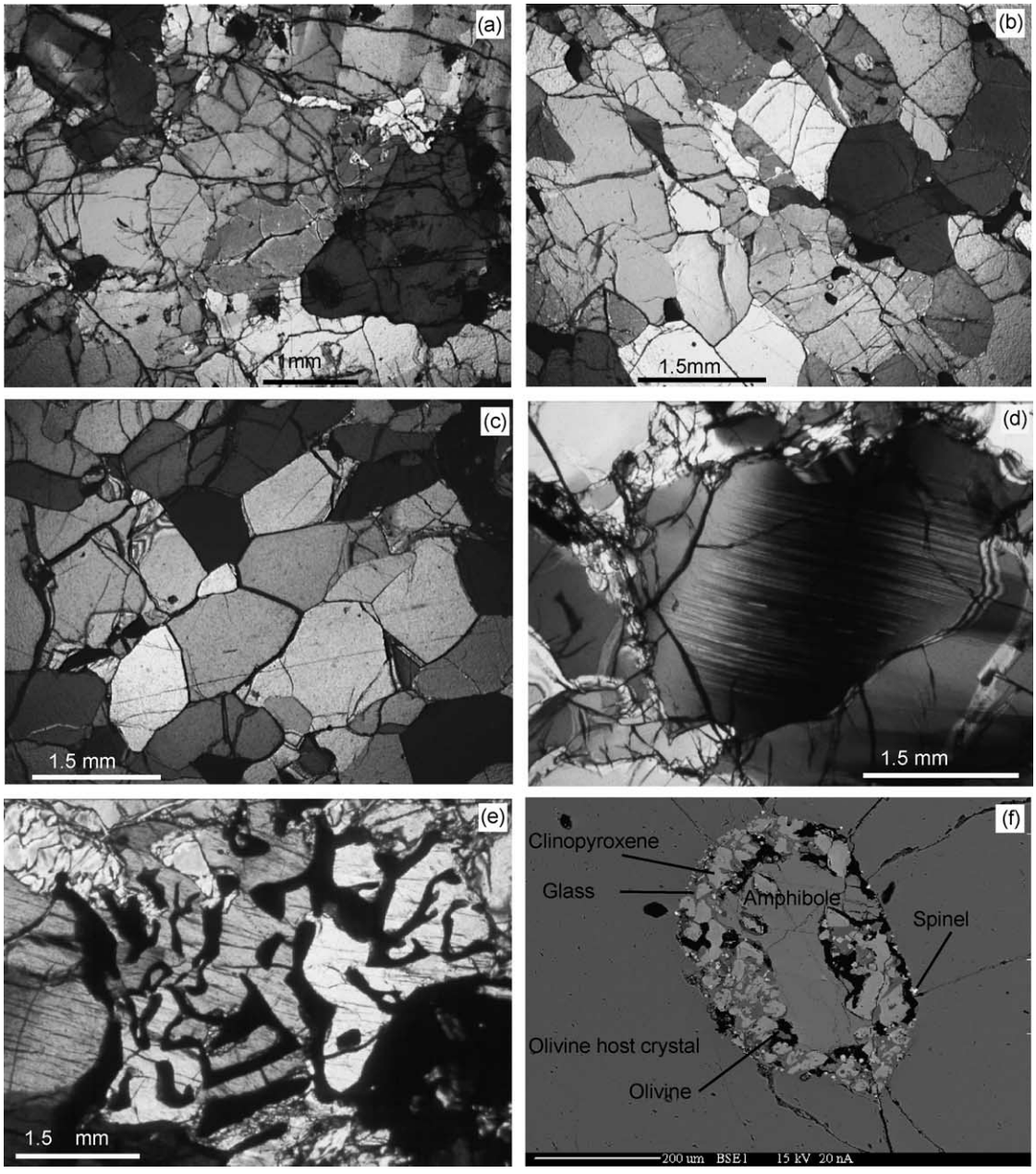

Fig. 2. (a) Porphyroclastic harzburgite from Prahuaniyeu. (b) Tabular equigranular harzburgite from Comallo. (c) Mosaic equigranular harzburgite from Comallo. (d) Orthopyroxene exsolutions in clinopyroxene crystal from Traful. (e) Pyroxene-Cr spinel symplectites from Laguna Fría. (f) Amphibole crystal hosted by an olivine crystal surrounded by glass, olivine, clinopyroxene, and spinel from Comallo. (g) Wehrlite from Gobernador Gregores with melt pocket (Sp, spinel; M, melt; Ol, olivine; Cpx, clinopyroxene; V, vesicle). (h) Mica plates crosscut by a metasomatic melt vein and surrounded by olivine crystals from Gobernador Gregores. (i) Garnet with narrow kelyphytic rim composed of orthopyroxene, clinopyroxene, and spinel. Garnet harzburgite from Prahuaniyeu.

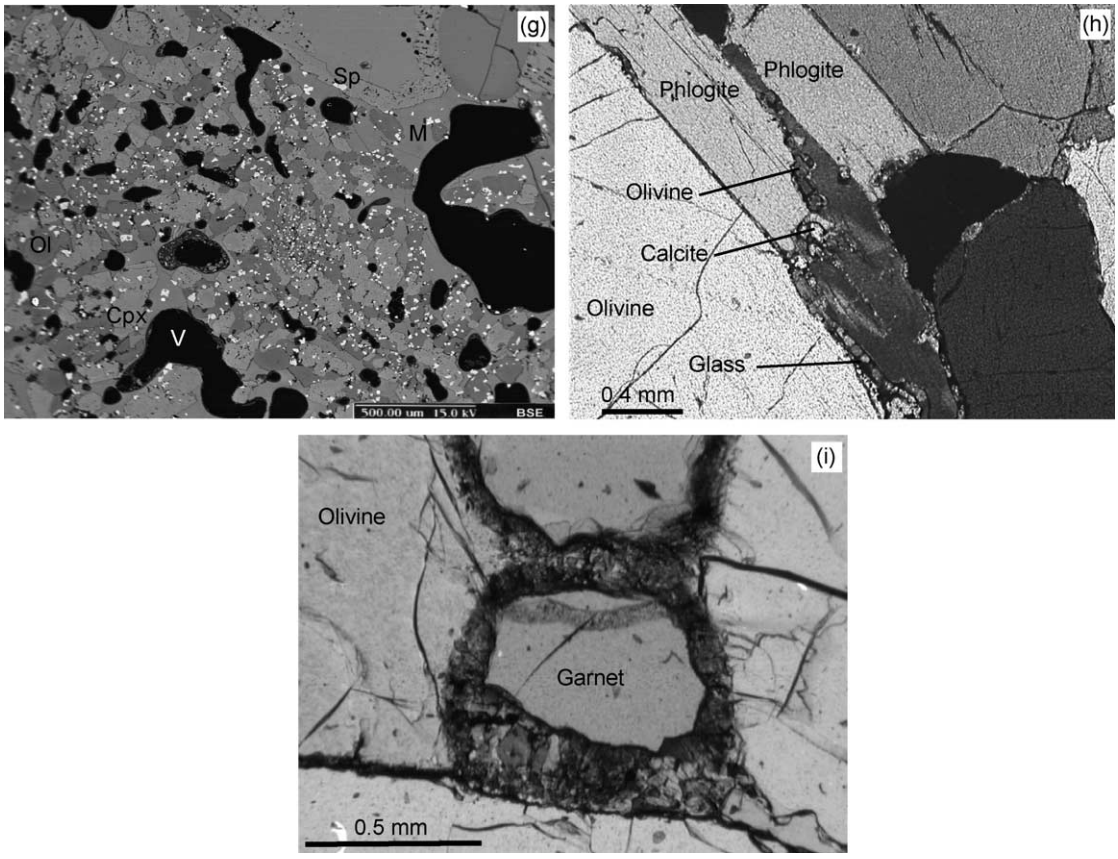

Fig. 2 (*continued*)

content varies from approximately 39 to 48 wt% and is correlated with most minor elements. With increasing MgO content, TiO_2, Al_2O_3, CaO, and Na_2O contents decrease. Approximately 60% of the xenoliths plot between 44 and 47 wt% MgO. Between this cluster and the composition of the primitive upper mantle is a mixing trend that, however, either has large scatter or consists of two separate trends. An example of the former is the CaO versus MgO trend (Fig. 3a); one of the latter is the Al_2O_3 versus MgO trend (Fig. 3b) in which one trend of Al_2O_3 ranges from 0.60 to 1.80 wt% and another ranges from 1.80 to 3.70 wt%. A double-mixing trend is also present in the CaO versus Al_2O_3 plot (Fig. 3e). A few peridotite compositions, mainly from Pali Aike and Gobernador Gregores, plot outside the trends.

Table 2
Electron microprobe analyses of amphibole (Amph) and phlogopite (Phl) from Patagonian xenoliths (wt%)

Mineral	Amph					Phl
Sample	DUB-2G	DUB-24	Co-19	Co-09	Co-1321	DUB-3G
SiO_2	44.7	42.7	43.93	43.0	41.62	38.6
TiO_2	2.20	3.50	1.33	2.22	1.90	2.8
Al_2O_3	11.6	13.6	14.09	13.93	15.08	15.7
Cr_2O_3	1.96	1.59	1.70	1.50	0.16	1.75
FeO[a]	4.5	4.5	3.28	4.64	7.3	5.6
MnO	0.05	0.08	0.06	0.06	0.09	0.03
NiO	0.09	0.03	0.1	0.13	0.08	0.16
MgO	18	17.1	18.5	17.2	16.28	20.9
CaO	9.9	10.2	11.67	11.45	11.21	0.03
BaO	n.a.	n.a.	n.a.	n.a.	n.a.	0.27
Na_2O	4.3	3.0	3.29	3.48	3.24	0.95
K_2O	1.31	1.69	0.70	0.90	n.a.	9.0
Total	98.61	97.99	98.65	98.52	96.96	95.79

Notes. n.a., not analyzed.
[a] Fe total as FeO.

Table 3
Major and trace element analyses of xenoliths from Patagonia

Rock	Sp-harzburgite							Websterite	Wehrlite	Sp-harz-burgite	Grt-lher-zolite
Sample	Co-26	LF-4	LF-9	Tr-10	Pr-1E	TL-18	PA-39	Ch-8	DUB-2G	PA-5	PA-24 Grt
XRF (wt%)											
SiO_2	44.32	44.47	45.37	43.92	n.a.	42.75	44.22	47.56	41.46	44.37	44.02
TiO_2	0.03	0.04	0.02	0.00	n.a.	0.05	0.07	0.03	0.22	0.30	0.34
Al_2O_3	2.28	2.32	2.50	2.06	n.a.	1.19	1.04	3.79	1.37	3.13	3.56
Fe_2O_3	8.22	8.49	8.22	8.44	n.a.	8.72	8.33	6.49	10.26	9.98	9.23
MnO	0.12	0.13	0.12	0.12	n.a.	0.12	0.11	0.12	0.15	0.12	0.13
MgO	45.10	44.13	43.15	45.58	n.a.	45.41	46.38	33.18	40.97	39.88	39.82
CaO	0.73	1.07	1.30	0.36	n.a.	0.61	0.35	9.69	3.15	1.50	2.24
Na_2O	0.04	0.04	0.02	0.02	n.a.	0.08	0.04	0.10	0.51	0.17	0.30
K_2O	0.02	0.01	n.a.	0.01	n.a.	0.15	0.09	n.a.	0.23	0.15	0.21
P_2O_5	0.04	0.03	0.02	0.02	n.a.	0.02	0.02	0.02	0.07	0.02	0.05
Total	100.90	100.73	100.72	100.53	⋯	99.10	100.65	100.98	99.54	99.62	99.90
Mg#	0.83	0.82	0.82	0.82	⋯	0.82	0.83	0.82	0.77	0.78	0.79
*INAA (ppm)−XRF (ppm)−**:XRF+INAA (ppm)*											
Sc**	6.40	8.07	10.10	5.99	10.90	7.44	6.72	20.60	8.8	11.90	12.80
Cr**	2233	2510	2645	2310	2876	3060	2450	3854	2940	2660	2390
Co**	110	101	106	112	109	125	113	79	107	119	97
Ni	2608	2520	2970	2490	2707	2340	2700	1530	2090	2080	1450
Zn	40	32	45	38	51	56	51	49	89.2	60	52
Ga	3.00	n.a.	3.00	3.00	n.a.	n.a.	n.a.	4.00	7.1	n.a.	n.a.
Rb**	n.a.	1.75	1.00	n.a.	n.a.	n.a.	1.10	2.00	n.a.	0.50	6.43
Sr	<5	<5	<5	<5	<5	<5	<5	<5	85.3	<5	<5
Y	3.00	<3	4.00	3.00	<3	<3	<3	5.00	3.6	<3	<3
Zr	11.00	25.50	7.00	7.00	n.a.	26.00	9.00	14.00	29.7	24.70	28.00
Nb	4.00	<3	4.00	4.00	<3	<3	<3	6.00	16.8	<3	<3
Ba**	<10	<10	<10	<10	<10	10.00	<10	<10	27.5	<10	21.00
La	0.26	0.74	0.53	0.12	0.84	0.40	0.76	0.45	2.9	0.46	2.83
Ce	0.65	2.41	1.29	0.29	2.06	0.87	1.14	1.06	9.12	1.94	5.22
Nd	n.a.	n.a.	n.a.	n.a.	n.a.	n.a.	0.77	n.a.	n.a.	n.a.	2.58
Sm	0.10	0.25	0.14	0.01	0.12	0.09	0.14	0.13	1.47	0.29	0.71
Eu	0.03	0.05	n.a.	0.01	0.02	0.02	0.04	0.05	0.44	0.06	0.22
Tb	n.a.	0.07	n.a.	n.a.	n.a.	0.02	0.02	n.a.	0.22	0.08	0.09
Yb	0.04	0.27	0.04	0.04	0.07	0.08	0.03	0.10	0.67	0.28	0.37
Lu	0.01	0.03	0.01	0.01	0.01	0.01	0.01	0.01	0.16	0.04	0.05
Hf	n.a.	0.13	n.a.	n.a.	n.a.	0.09	0.21	n.a.	1.77	0.24	0.46
Ta	n.a.	0.06	n.a.	n.a.	n.a.	0.07	0.13	n.a.	1.11	0.10	0.37
Th	n.a.	0.14	n.a.	n.a.	n.a.	0.14	0.07	n.a.	0.18	0.05	0.23
U	n.a.	0.06	n.a.	n.a.	n.a.	0.59	0.07	n.a.	0.40	0.11	0.07
La/Yb	6.5	2.7	13.25	3.0	12	5.0	25.3	4.5	4.3	1.6	7.6

Notes. n.a., not analyzed.

Trace element abundances (Table 3, Fig. 3c,d) commonly covary with the MgO content; abundances decrease with increasing MgO content (except Ni and Co, whose contents increase).

6.2. Rare earth elements

Rare earth element abundance patterns (Fig. 4) in peridotites from Comallo display low HREE abundances (∼0.2×CI) and slight LREE enrichment (∼1.2×CI) over the HREE. Xenoliths from Laguna Fría show two different trends, both of which have low (∼0.2–0.5×CI) HREE abundances, but one has low LREE abundances (∼0.2–0.4×CI, flat pattern), whereas the other has high LREE abundances (∼2–4×CI). Only one peridotite (LF-4) has a flat REE abundance pattern at ∼1–2×CI. Peridotites from Traful are all HREE poor (∼0.1–0.3×CI) and slightly enriched in LREE over HREE (∼0.2–0.9×CI). Peridotites from Chubut show a similar trend, but the LREE commonly is more strongly enriched over the HREE (∼2–5×CI). Two rocks from Tres Lagos have flat patterns with chondritic REE abundances. Spinel peridotites from Pali Aike show the largest variability in HREE abundances (∼0.1–2×CI) and are mostly LREE enriched over the HREE (∼0.6–7×CI). One garnet-bearing peridotite from Pali Aike (PA-24 Grt) has a similar REE pattern but overall higher abundances (∼1 and 10×CI for HREE and LREE, respectively), whereas the other has a flat REE pattern at ∼1×CI. A spinel-bearing peridotite from Gobernador Gregores (DUB-3G) has a REE pattern similar to that of PA-24 Grt.

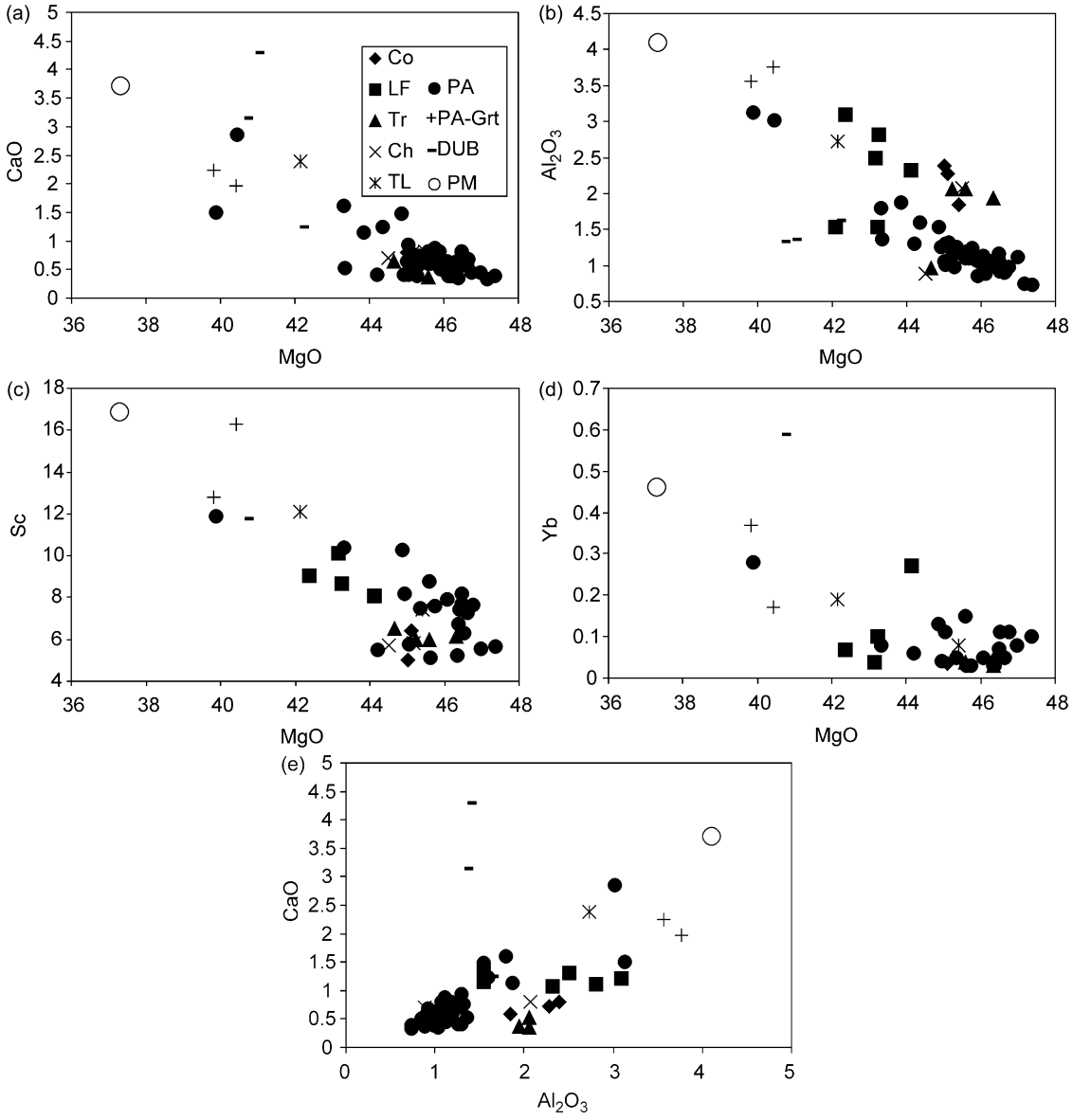

Fig. 3. (a–d) Variation of bulk major oxides (wt%) and trace elements (ppm) against MgO for Patagonia xenoliths. (e) Variation of bulk Al_2O_3 (wt%) against CaO (wt%). PA-Grt, Pali Aike garnet-bearing xenoliths; PM, primitive mantle (Sun and McDonough, 1989).

7. Mineral chemistry

7.1. Major and minor elements

We provide representative analyses of selected minerals in Tables 4A–D and include a detailed description of the mineral chemistry of the studied localities in Appendix 1. Olivine composition (Table 4A) ranges between Fo 90 and Fo 92 (mole%) in spinel- and garnet-bearing lherzolites and harzburgites. The Fo mean value is 84 mole% for websterites but 92 mole% in websterites from composite xenoliths. CaO contents of olivines are 0.03–0.19 wt%, and NiO contents are approximately 0.4 wt%. Websterite Co-13 olivine has low NiO content and is rich in FeO and CaO.

Orthopyroxene average compositions (Table 4B) are in the range $En_{90–91}$ Wo_1 $Fs_{8–9}$ in harzburgites (including spinel- and garnet-bearing types), $En_{88–90}$ $Wo_{1–3}$ Fs_9 in lherzolites (both spinel- and garnet-bearing types), En_{80} Wo_2 Fs_{18} in spinel-bearing websterites, En_{90} Wo_1 Fs_9 in wehrlite, and En_{90} Wo_2 Fs_8 in websterite veins from composite lherzolites. Minor element contents vary widely: TiO_2 $<0.02–1.00$ wt% (websterites), Al_2O_3 1.86–5.63 wt%, Cr_2O_3 0.05–0.79 wt%, and CaO 0.43–1.51 wt%.

Clinopyroxene mean compositions (Table 4C) are in the range $En_{47–51}$ $Wo_{41–50}$ $Fs_{3–5}$ in harzburgites (including spinel- and garnet-bearing types), $En_{48–52}$ $Wo_{42–48}$ $Fs_{4–6}$ in lherzolites (both spinel- and garnet-bearing types), $En_{44–48}$ $Wo_{46–49}$ $Fs_{3–10}$ in spinel-bearing websterites, En_{51} Wo_{43} Fs_6 in wehrlites, and En_{48} Wo_{49} Fs_3 in websterites veins in

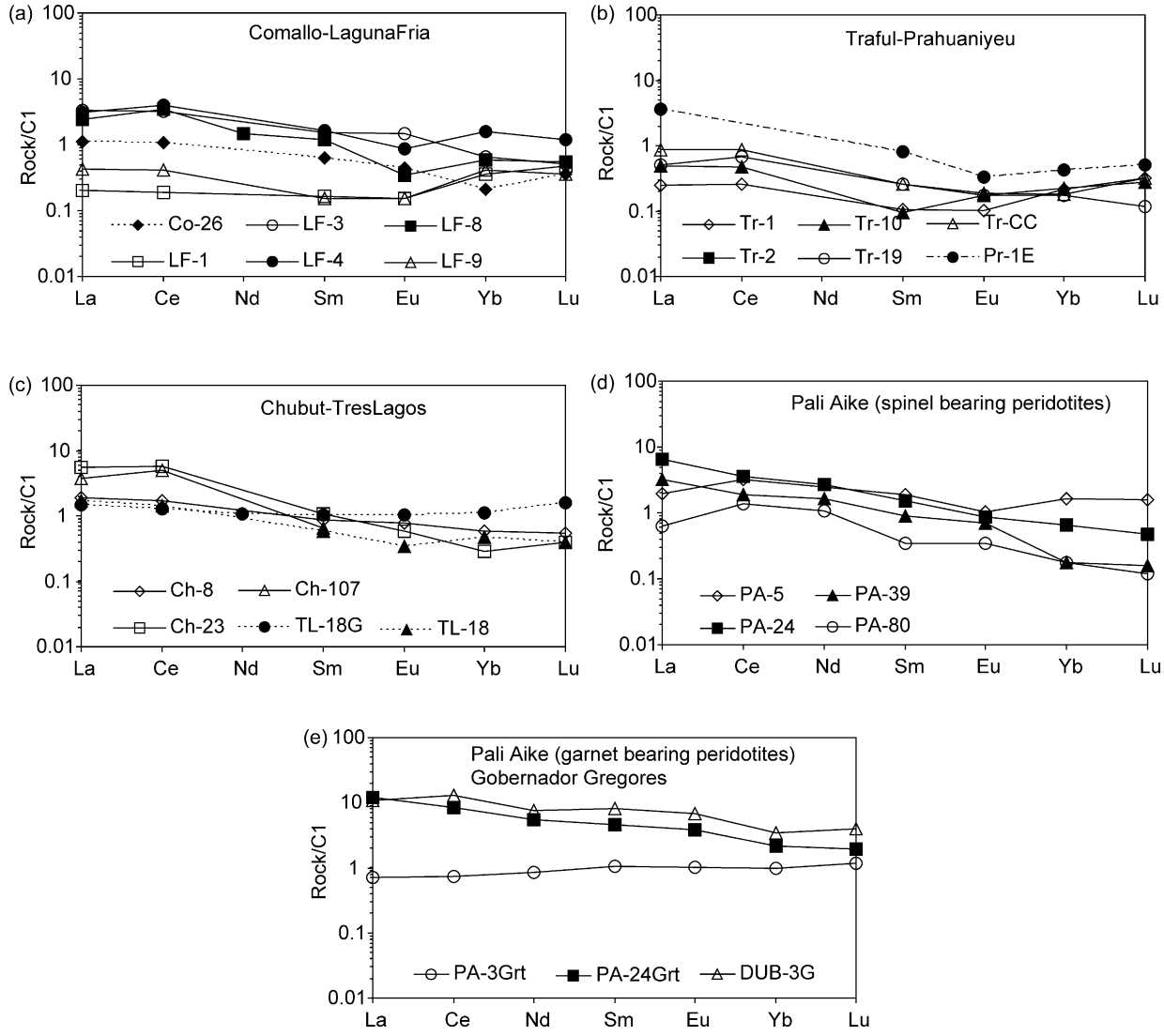

Fig. 4. Chondrite-normalized bulk REE concentration patterns of representative Patagonia xenoliths (Grt, garnet-bearing samples). Chondrite normalizing values from Sun and McDonough (1989).

composite xenoliths. Minor element contents vary over a wide range: TiO_2 <0.02–1.5 wt%, Cr_2O_3 0.08–1.7 wt%, and Na_2O 0.30–1.74 wt%. Some elements display a rough correlation (e.g. Na_2O versus Al_2O_3, some TiO_2 versus Al_2O_3); however, Cr_2O_3 and Al_2O_3 are totally independent of each other.

The mg# and cr# for spinels (Table 4D) are in the range, respectively, 69–75 and 32–45 in harzburgites (including spinel- and garnet-bearing), 78–79 and 12–21 in lherzolites (spinel- and garnet-bearing), 41–43 and 55–56 in wehrlites, 66 and 2 in websterites, and 71 and 40 in websterites veins in composite xenoliths.

Garnet compositions (Table 4D) in spinel-bearing lherzolites and harzburgites are as follows: pyrope 73–74, almandine 13–12, grossular 9–4, andradite 0–4, uvarovite 5, and spessartine 1. Symplectite mineral phases display a narrow compositional range (orthopyroxene $En_{91–92}$ Wo_1 Fs_8, clinopyroxenes $En_{50–54}$ $Wo_{41–47}$ $Fs_{3–5}$), and spinel mg# and cr# vary between 70–73 and 40–7, respectively.

7.2. Rare earth elements in clinopyroxenes

Clinopyroxenes from selected Patagonian xenoliths (Table 5, Fig. 5) display several distinct REE patterns. Those from the northern part of Patagonia (north of 44°S) have low HREE contents (~0.5–3×CI) and three different patterns. One (Co-32) has high MREE abundances with a hump at Nd and lower abundances of LREE and HREE (Fig. 5a). The second trend is complementary, with low MREE and higher LREE and HREE (LF-1). The third trend has almost flat HREE and steeply increasing LREE abundances (LF-4, Tr-10).

Samples from southern Patagonia (south of 44°S) have clinopyroxene REE patterns different from those in

Table 4A
Representative electron microprobe analyses of olivines in xenoliths from Patagonia (wt%)

Rock	Sp-harzburgite					Grt-lherzolite	Grt-harzburgite	Websterite	Wehrlite
Sample	Co-26	LF-9	Tr-10	Pr-09	TL-18	Pr-99	PA-24	Co-13	DUB-2G
SiO_2	41.0	41.2	41.3	41.0	41.0	41.2	40.8	39.9	40.7
TiO_2	<0.02	<0.02	<0.02	<0.02	<0.02	<0.02	<0.02	<0.02	<0.02
Al_2O_3	<0.02	<0.02	<0.02	<0.02	<0.02	<0.02	<0.02	<0.02	<0.02
Cr_2O_3	<0.02	<0.02	<0.02	<0.02	<0.02	<0.02	<0.02	<0.02	<0.02
FeO[a]	8.2	8.9	8.3	8.2	9.1	9.1	9.2	15.1	9.5
MnO	0.12	0.14	0.08	0.12	0.14	0.12	0.15	0.25	0.14
NiO	0.39	0.41	0.38	0.38	0.36	0.39	0.38	0.11	0.39
MgO	50.5	49.4	50.9	50.3	49.8	48.5	49.1	44.3	49.8
CaO	0.07	0.19	0.04	0.07	0.13	0.11	0.17	0.25	0.03
Total	100.39	100.21	101.02	100.13	100.7	99.42	99.89	99.83	100.47
Fo[b]	91.6	90.8	91.6	91.6	90.5	90.9	91.2	83.9	90.33

[a] Fe total as FeO.
[b] Fo: mole% forsterite.

Table 4B
Representative electron microprobe analyses of orthopyroxenes in xenoliths from Patagonia (wt%)

Rock	Sp-harzburgite					Grt-lherzolite	Grt-harzburgite	Websterite	Wehrlite
Sample	Co-26	LF-9	Tr-10	Pr-09	TL-18	Pr-99	PA-24	Co-13	DUB-2G
SiO_2	56.5	56.0	57.3	56.7	56.2	54.8	55.4	53.0	55.4
TiO_2	0.05	<0.02	<0.02	<0.02	0.07	0.15	0.15	1.01	0.25
Al_2O_3	2.41	3.1	1.86	2.37	3.5	5.63	3.9	5.0	3.6
Cr_2O_3	0.47	0.50	0.40	0.48	0.31	0.79	0.54	0.05	0.33
FeO[a]	5.3	5.3	5.3	5.2	5.8	5.72	6.2	10.8	6.0
MnO	0.13	0.12	0.11	0.12	0.14	0.11	0.13	0.23	0.14
NiO	0.10	0.12	0.09	0.09	0.10	0.11	0.09	0.06	0.09
MgO	34.9	34.1	35.3	35.0	34.4	30.9	33.5	29.5	34.0
CaO	0.64	1.51	0.43	0.50	0.51	1.30	0.56	0.84	0.48
Na_2O	<0.02	0.06	0.07	0.12	0.05	0.19	0.06	<0.02	0.05
Total	100.51	100.78	100.8	100.53	101.07	99.7	100.56	100.59	100.42
En	91	90	91	91	90	88	90	83	90
Fs	8	8	8	8	9	9	9	17	9
Wo	1	2	1	1	1	3	1	2	1

[a] Fe total as FeO.

Table 4C
Representative electron microprobe analyses of clinopyroxenes in xenoliths from Patagonia (wt%)

Rock	Sp-harzburgite					Grt-lherzolite	Grt-harzburgite	Websterite	Wehrlite
Sample	Co-26	LF-9	Tr-10	Pr-09	TL-18	Pr-99	PA-24	Co-13	DUB-2G
SiO_2	53.0	52.8	54.1	53.9	52.6	52.3	52.2	49.9	50.8
TiO_2	0.27	<0.02	<0.02	<0.02	0.38	0.35	0.51	0.66	1.55
Al_2O_3	3.3	3.8	2.09	1.94	5.6	6.73	5.1	6.4	6.8
Cr_2O_3	1.12	1.11	0.97	0.98	0.82	1.26	1.07	0.08	0.88
FeO[a]	2.32	2.8	2.3	2.02	2.29	3.21	2.46	5.3	2.13
MnO	0.07	0.07	0.02	0.07	0.08	0.10	0.08	0.13	0.07
NiO	0.05	0.07	0.06	0.06	0.04	0.06	0.05	0.03	0.04
MgO	17.2	18.6	18.3	17.8	15.9	16.12	15.9	14.9	14.8
CaO	22.2	20.4	22.4	22.9	21.9	18.03	21.6	21.8	21.2
Na_2O	0.83	0.42	0.46	0.61	1.20	1.39	1.22	0.61	1.55
Total	100.35	100.09	100.7	100.24	100.72	99.55	100.25	99.85	99.84
En	50	53	51	50	48	52	48	44	47
Fs	4	5	4	3	4	6	4	9	4
Wo	46	42	45	47	48	42	48	47	49

[a] Fe total as FeO.

Table 4D
Representative electron microprobe analyses of spinels and garnets in xenoliths from Patagonia (wt%)

Mineral	Spinel									Mineral	Garnet	
Rock	Sp-harzburgite					Grt-lher-zolite	Grt-harz-burgite	Webster-ite	Wehrlite	Rock	Grt-harz-burgite	Grt-lher-zolite
Sample	Co-26	LF-9	Tr-10	TL-18	Pr-09	Pr-99	PA-24	Co-13	DUB-2G	Sample	PA-24	Pr-99
SiO_2	0.06	0.14	0.02	0.06	0.04	0.13	0.12	0.07	0.04	SiO_2	42.4	42.33
TiO_2	0.18	<0.02	<0.02	0.06	<0.02	0.32	1.36	0.34	0.24	TiO_2	0.23	0.21
Al_2O_3	33.7	42.0	30.5	57.2	40.0	48.91	34.5	60.1	55.2	Al_2O_3	22.8	22.9
Cr_2O_3	36.0	25.9	40.5	11.4	30.1	19.06	30.5	1.46	12.4	Cr_2O_3	1.67	1.70
Fe_2O_3	1.20	2.7	2.00	1.30	1.00	1.23	3.9	5.1	1.10	Fe_2O_3	1.44	<0.02
FeO	11.4	9.0	11.1	8.6	11.1	9.92	12.2	14.8	9.3	FeO	5.9	6.45
MnO	0.12	<0.02	<0.02	<0.02	<0.02	0.07	<0.02	0.09	0.00	MnO	0.32	0.29
NiO	0.21	0.30	0.18	0.39	0.21	0.37	0.33	0.22	0.36	NiO	0.02	0.03
MgO	16.88	19.2	17.0	21.1	17.8	19.38	17.3	17.5	20.3	MgO	21.3	20.6
										CaO	5.1	5.3
										Na_2O	0.04	<0.02
Total	99.69	99.31	101.3	100.14	100.25	99.39	100.2	99.69	98.95	Total	101.22	99.8
Mg#	72.2	78.6	72.7	80.7	73.8	77.62	71	67.3	78.9	py	74	73.1
Cr#	41.2	28.4	46.1	11.6	33.2	20.72	35.6	1.5	12.9	alm	12	12.8
										gro	4	8.7
										and	4	0
										uv	5	4.7
										sp	1	0.7

Notes. En, enstatite; Fs, ferrosilite; Wo, wollastonite. mg# is (MgO/MgO + FeO) × 100 in moles, and cr# is (Cr_2O_3/(Cr_2O_3 + Fe_2O_3 + Al_2O_3) × 100 in moles. py, pyrope; alm, almandine; gro, grossular; and, andradite; uv, uvarovite; sp, spessartine.

the north. The clinopyroxenes from Gobernador Gregores (Fig. 5b) have low HREE contents (~1 × CI) with strongly increasing abundances of MREE and LREE (Lu to Ce from ~1 to 38 × CI) and a slight depletion in La with respect to Ce (DUB-3G). Clinopyroxenes from Tres Lagos (TL-18 and TL-18G) xenoliths (Fig. 5b) have high HREE contents (~6 × CI) and depleted LREE with respect to HREE (La ~0.1–0.6 × CI). In Pali Aike (Fig. 5c), clinopyroxenes from spinel harzburgites have similar REE patterns to those from Tres Lagos but with a slight reverse trend for LREE (PA-3 and PA-8). Another group of spinel-bearing xenoliths has low HREE (~1 × CI), increasing abundances of MREE (Lu to Sm from ~1 to 5 × CI), and decreasing abundances of LREE (Nd to La ~5 to 3–1.7 × CI). Clinopyroxene from a garnet-bearing peridotite (PA-A) is poor in HREE, has increasing MREE abundances (Lu to Sm ~0.4–4 × CI), and has slightly decreasing abundances of LREE (La ~1 × CI). The coexisting garnet (PA-A Grt) has high HREE contents (~14 × CI) and decreasing abundances of MREE and LREE (La ~0.03 × CI).

Table 5
Representative LA-ICP-MS analyses of REE in clinopyroxenes and garnet (in ppm)

Sample	La	Ce	Pr	Nd	Sm	Eu	Gd	Tb	Dy	Ho	Er	Tm	Yb	Lu
Co-32	1.97	9.14	1.65	9.08	2.88	0.97	2.76	0.42	2.26	0.42	1.00	0.13	0.66	0.10
LF-1	0.12	0.20	0.01	0.06	0.02	0.01	0.06	0.02	0.21	0.07	0.28	0.05	0.47	0.07
LF-4	14.97	28.56	2.52	6.34	0.70	0.20	0.47	0.07	0.49	0.12	0.39	0.06	0.50	0.08
Tr-10	3.45	5.36	0.45	1.16	0.19	0.05	0.09	0.03	0.12	0.03	0.14	0.02	0.14	0.02
DUB-3G	11.84	36.09	5.44	24.08	6.52	2.16	5.24	0.78	3.30	0.50	0.98	0.11	0.47	0.06
TL-18	0.24	1.71	0.38	2.43	1.17	0.52	1.75	0.38	2.62	0.60	1.65	0.26	1.62	0.24
TL-18G	0.05	0.70	0.22	1.64	1.08	0.36	1.27	0.28	1.85	0.43	1.34	0.22	1.26	0.18
PA-A Grt	0.01	0.05	0.03	0.42	0.53	0.37	1.80	0.51	4.12	1.03	3.38	0.51	3.22	0.55
PA-A	0.35	1.72	0.42	2.46	0.95	0.37	1.22	0.20	0.93	0.15	0.32	0.04	0.24	0.03
PA-3	0.09	0.28	0.06	0.52	0.27	0.12	0.63	0.16	1.21	0.27	0.84	0.14	0.83	0.13
PA-2	0.62	1.99	n.a.	2.96	1.60	0.54	1.42	0.26	n.a.	n.a.	n.a.	n.a.	0.55	0.06
PA-5	1.48	7.65	n.a.	4.90	1.85	0.68	2.00	0.40	n.a.	n.a.	n.a.	n.a.	0.77	0.10
PA-7	1.11	3.46	n.a.	3.60	1.20	0.46	1.32	0.26	n.a.	n.a.	n.a.	n.a.	0.34	0.04
PA-8	0.81	4.04	n.a.	3.40	1.05	0.37	n.a.	0.26	n.a.	n.a.	n.a.	n.a.	1.04	0.20
PA-13	2.63	9.15	n.a.	4.51	1.63	0.58	n.a.	0.27	n.a.	n.a.	n.a.	n.a.	1.13	0.20

Notes. n.a., not analyzed.

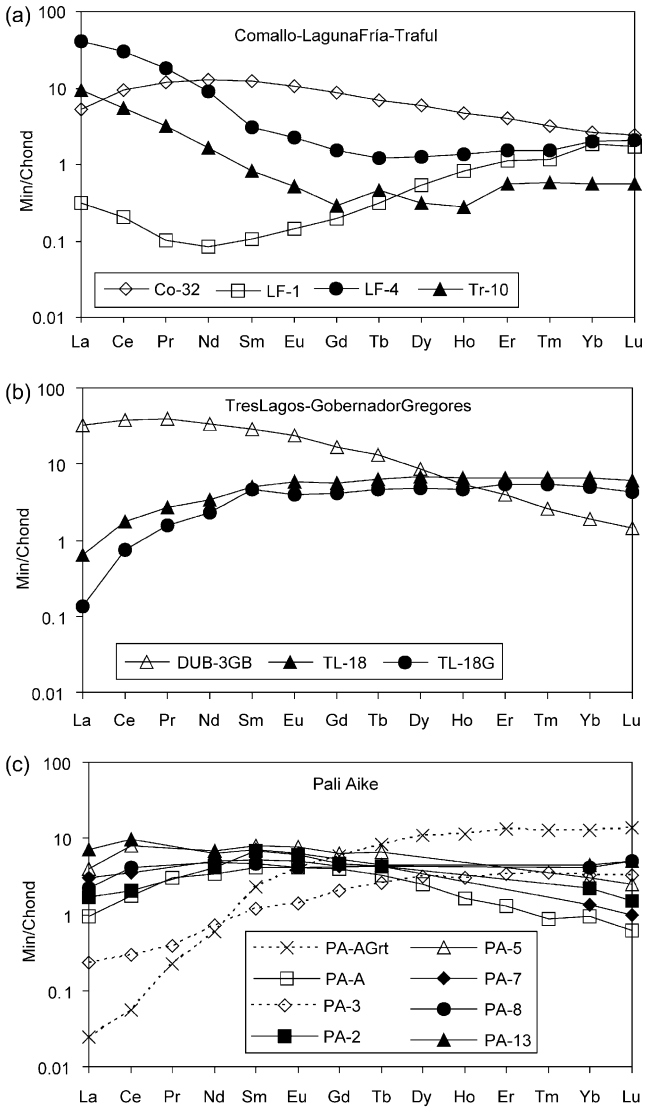

Fig. 5. LA-ICP-MS chondrite-normalized clinopyroxene REE concentration patterns of selected Patagonian xenoliths (Grt, garnet-bearing samples). Chondrite normalizing values from Sun and McDonough (1989).

8. Discussion

8.1. The depleted upper mantle in Patagonia

Peridotites of primitive chemical composition are lacking in Patagonia, and only a few from the south approach that composition. In northern Patagonia (41°–44°S), xenoliths depleted in a basaltic component dominate. The Al_2O_3–CaO diagram (Fig. 3e) shows that Patagonian xenoliths define two positively correlated parallel trends, with xenoliths from northern Patagonia displaying lower contents of both CaO and Al_2O_3 than those from the south.

The most fertile xenoliths occur in southern Patagonia (Fig. 3e). However, these rocks are rare and heavily dominated by rocks strongly depleted in basaltic component. This trend is evident for both the Pali Aike garnet-bearing xenoliths and the Tres Lagos and Gobernador Gregores samples. Fig. 3a–d demonstrates that CaO, Al_2O_3, Yb, and Sc are anticorrelated with MgO, which is a good indicator of the varying depletion of basaltic components in the mantle (Frey et al., 1985; McDonough, 1990).

The MgO–Al_2O_3 diagram (Fig. 3b) shows one trend for the most refractory xenoliths and another trend for somewhat more fertile xenoliths. These trends probably reflect minor melt extraction in the deeper upper mantle and extensive extraction in the shallower upper mantle, respectively, because Al partitions into the melt more strongly from spinel peridotite than from garnet peridotite (Walter and Presnall, 1994).

Small bulk mg# variations and the Ni abundance indicate that the xenoliths are partial melting residues. The CaO, Al_2O_3, and Lu abundances are anticorrelated with bulk mg#, consistent with the extraction of partial melts from a primitive source.

Correlation diagrams of spinel cr# and Al in coexisting orthopyroxene and clinopyroxene (Fig. 6) show that tectonized xenoliths are more refractory and that Al in clinopyroxene decreases with increasing cr# in spinel more rapidly than does Al in coexisting orthopyroxene. This finding is consistent with the observation that clinopyroxene is consumed before other phases during partial melting and explains the preponderance of harzburgites in Patagonia.

8.2. Metasomatic events

In Patagonian upper mantle xenoliths, bulk-rock and mineral analyses indicate extensive elemental depletions in the garnet and spinel peridotite stability fields. In addition, modal and cryptic metasomatic enrichments events are recorded in many rocks.

8.2.1. Modal metasomatism

In northern Patagonia, samples from the westernmost locality, Comallo, are depleted in HREE and enriched in LREE ($La_N/Yb_N \cong 5$, Fig. 4a, Table 3), a clear sign of metasomatic events that led to the addition of incompatible elements and was accompanied by the formation of glass veins and amphibole.

In Prahuaniyeu, xenoliths show almost chondritic HREE contents and LREE enrichment, with a La_N/Yb_N ratio maximum value of $\cong 9$ (Fig. 4b, Table 3). The bulk REE patterns of spinel-bearing xenoliths (Ntaflos et al., 2001, 2002) plot parallel to the clinopyroxene REE patterns, and both are strongly enriched in LREE, as indicated by $(La_N/Yb_N)_{bulk} = 8$ and $(La_N/Yb_N)_{cpx} = 16$. Modal metasomatism is documented by the presence of phlogopite, glass veins, and, in garnet-bearing harzburgites, melt pockets composed of glass, spinel, olivine, and clinopyroxene.

South of 44°S, xenoliths are more variable in their REE contents than are their northern counterparts. Tres Lagos

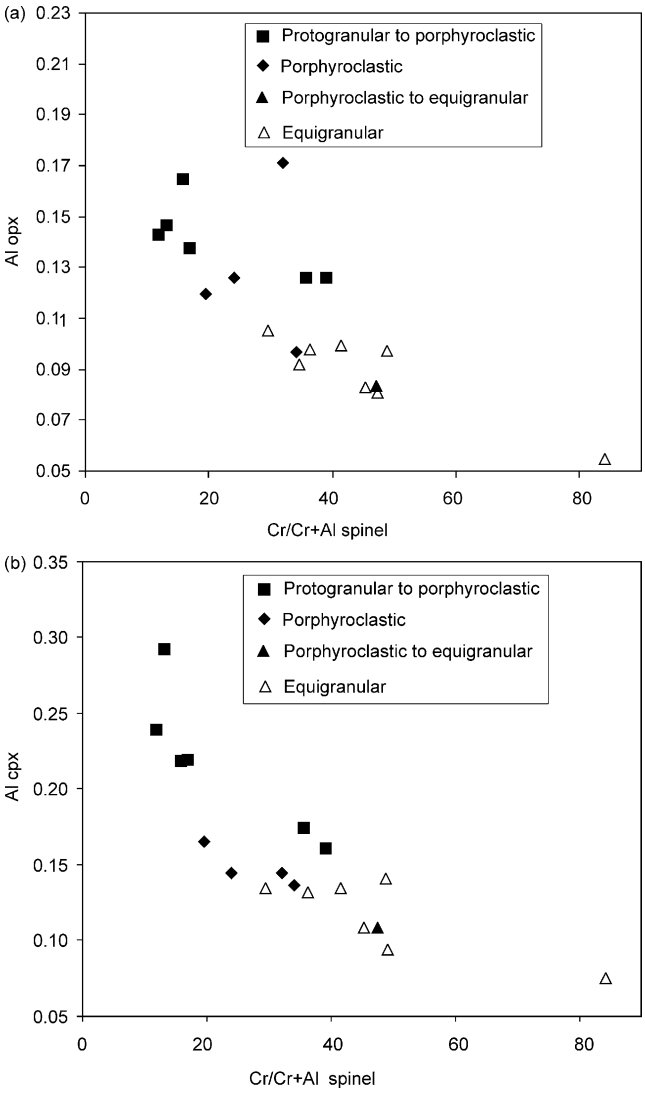

Fig. 6. Correlation diagram, with indication of xenolith texture, spinel cr#, and Al in coexisting (a) orthopyroxene and (b) clinopyroxene.

samples comprise one group with almost chondritic REE contents and another that displays HREE depletion and four times the chondrite LREE enrichment with La_N/Yb_N ratios up to 3 (Fig. 4c, Table 3). These xenoliths all carry glass veins. Gobernador Gregores xenoliths are all metasomatized. Hydrous phases (phlogopite, amphibole), melt pockets, and glass veins document the activity of hydrous fluids and melts (Ntaflos et al., 1998, 1999; Dobosi et al., 1999). These fluids caused enrichments of both HREE (2–8×CI) and LREE (La_N/Yb_N ratios range from 5 to 18).

Green chromian diopside has a spongy envelope consisting of intergrowths of pale-green clinopyroxene (cpx) and a brownish melt, indicating reaction with fluids or melts. Fine-grained spinel (sp) was found only as inclusion in olivine (ol) and forms trails along the boundary with melt pockets. Disseminated dark phlogopite plates (Fig. 2h) and pargasitic amphiboles are affected by the same fluids or melts, which caused the clinopyroxene breakdown. However, anhydrous xenoliths commonly have moderately depleted HREEs (0.2–0.8×CI) and LREE enrichments with La_N/Yb_N ratios ranging from 2 to 3 (Table 3, Fig. 4).

Garnet-bearing harzburgites (PA-3 Grt) from Pali Aike have an almost chondritic REE pattern, whereas garnet lherzolites (PA-24 Grt) display a pronounced LREE enrichment, similar to that of the metasomatized wehrlites from Gobernador Gregores (Fig. 4e, Table 3). Spinel lherzolites from Pali Aike are characterized by chondritic REE abundances with $La_N/Yb_N \cong 1$, whereas spinel harzburgites show almost chondritic HREE contents but slight to moderate LREE enrichments, with $La_N/Yb_N \cong 5$ (Fig. 4d, Table 3). Modal metasomatism (Stern et al., 1999) is documented by the presence of phlogopite.

There is a positive correlation between LREE-enriched abundance patterns of whole rock and clinopyroxene for the localities, except for samples from Tres Lagos (Figs. 4 and 5). Whole-rock analyses of two samples (TL-18 and TL-18G) from this locality display the same absolute content of LREE, but TL-18 shows a slight enrichment in those elements ($La_N/Yb_N \cong 4$). Clinopyroxene analyses, in contrast, reveal a strong LREE depletion relative to MREE and HREE, which suggests they are preexisting, relict clinopyroxenes that record the trace element depletion event preceding the metasomatism event. This example suggests that melts introduced by the metasomatizing agent (now present as glass), not a melt formed in situ, produced the bulk LREE enrichment. The same process was postulated by Kilian and Stern (2002) for xenoliths from Cerro del Fraile, Santa Cruz.

8.2.2. Cryptic metasomatism

The whole-rock REE patterns from northern Patagonia show characteristic HREE depletion and variable LREE and MREE enrichments (Fig. 4a,b). Because hydrous phases and glass veins are absent in the studied xenoliths, it is obvious that they have experienced cryptic metasomatism. This conclusion is supported because the cpx REE patterns from the same samples show LREE enrichments (Fig. 5a). The samples from Laguna Fría fall into two groups, both with similar depleted HREE contents, that show different degrees of LREE enrichment. In one group, the La_N/Yb_N ratio ranges between 0.5 and 1, and they are depleted in MREE. The other group is LREE enriched (La_N/Yb_N between 2 and 5, maximum 9.6, Table 3), which reflects cryptic metasomatism (Fig. 4a).

Samples from Traful display features similar to those of the most depleted samples from Laguna Fría, namely, depletion of MREE and a La_N/Yb_N ratio in the 1–4 range (Fig. 4b, Table 3). Samples from Chubut (Fig. 4c) are depleted in HREE and exhibit LREE enrichment with La_N/Yb_N ratios up to 19.

8.2.3. Partial melting and metasomatism

The most refractory xenoliths display the highest La abundances and La/Yb ratios, in contrast with a one-stage

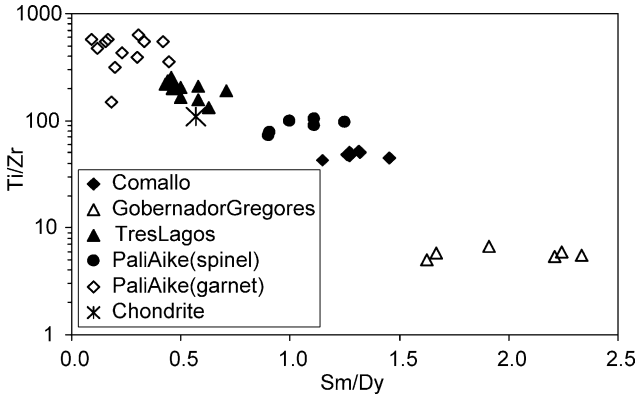

Fig. 7. Partial melting increases Ti:Zr ratio to >300. Addition of metasomatic component decreases the Ti:Zr ratio (Blusztajn and Shimizu, 1994). Chondrite values from Sun and McDonough (1989).

solid/liquid separation history. This evidence the introduction of mantle-related melts/fluids rich in LREE, which are mainly contained in minerals, as also is demonstrated by the common LREE enrichment of clinopyroxene (Fig. 5). Partial melting processes and the addition of metasomatic fluids/melts also is evidenced by trace element ratios. Clinopyroxenes from xenoliths of those localities where the most primitive samples occur (Fig. 7) have Ti:Zr ratios higher than the chondritic ratio (110); therefore, they are residues left after partial melting (Blusztajn and Shimizu, 1994). The clinopyroxenes in the remaining Patagonia xenoliths have Ti:Zr ratios lower than the chondritic ratio because the ratio decreases with the addition of a metasomatic component, regardless of the increasing effect that partial melting has on the Ti:Zr ratio of the residues.

8.3. Tectonics, mineral chemistry, and metasomatism

Different textural types of xenoliths are randomly distributed in Patagonia and indicate that the sublithospheric mantle is mildly to strongly tectonized on both a local and a regional scale and contains a clear predominance of deformed textural rock types.

The composition of olivines does not correlate with their texture, and their mg# display a limited range. In the same thin section, porphyroclast and neoblast olivines have nearly identical compositions, and no significant zoning appears in any of the analyzed grains. Spinel cr# is highest in the most tectonized xenoliths (>40), whereas those of spinels of the transitional textural types typically are <35.

A direct relationship between the degree of tectonism and cryptic metasomatism cannot be established because spinel harzburgites with quite different textures, from the same and different localities, display LREE enrichment in some samples, whereas others are depleted or only slightly enriched. Other than in the xenoliths from Gobernador Gregores, modal metasomatism is a feature that relates to the degree of tectonization; namely, it prevails in samples with equigranular (tabular and mosaic) textures.

8.4. Equilibrium conditions

For internal consistency, we used the two-pyroxene thermometer (Brey and Köhler, 1990) for the temperature estimation. For spinel peridotites, the only reliable barometer uses the Ca exchange between coexisting olivine and clinopyroxene (Köhler and Brey, 1990). To avoid the known analytical problems due to the low concentrations of Ca (<1.00 wt%) in olivine (Köhler and Brey, 1990; Dalton and Lane, 1996), we separated grains from several samples for microprobe analyses.

Estimated equilibrium *P–T* conditions for xenoliths from Comallo, Laguna Fría, Traful, Prahuaniyeu, Chubut, Tres Lagos, and Pali Aike are summarized in Table 6. The olivine-orthopyroxene and clinopyroxene grains used for the calculations are homogeneous, and the calculated equilibration temperatures vary from 1260 to 850 °C at 24–6 kbar.

Among the Patagonian mantle xenoliths, the garnet lherzolites from Pali Aike yield the highest temperatures with values around 1260 °C (Brey and Köhler, 1990) at 24 kbar. This pressure was calculated using barometers based on the Al contents of orthopyroxene coexisting with garnet (Brey and Köhler, 1990) and on the Ca content in olivine coexisting with clinopyroxene (Köhler and Brey, 1990). Both barometers yield the same pressure of 24 kbar. Calculated equilibration conditions for garnet lherzolites from Prahuaniyeu are in the range 1200–1216 °C

Table 6
Equilibration temperature and pressure estimates after Köhler and Brey (1990) and Brey and Köhler (1990)

Locality	*T* (°C)	*P* (kbar)	Description
Co-26	949	22	Sp-harzburgite
Co-30	975	19	Sp-harzburgite
LF-4A	1248	21	Sp-harzburgite
LF-4A1	1253	24	Sp-harzburgite
LF-9	1237	19	Sp-harzburgite
Tr-2	1125	17	Sp-harzburgite
Tr-2A	1137	23	Sp-harzburgite
Tr-8	1180	20	Sp-harzburgite
Pr-199	1216	23	Grt-lherzolite
Pr-91	1017	28	Sp-lherzolite
Pr-99	1200	24	Grt-lherzolite
Pr-96	1122	17	Sp-harzburgite
Ch-16A	1030	19	Sp-harzburgite
DUB-10	1090	13	Sp-lherzolite
DUB-30	830	12	Sp-lherzolite
DUB-1G	1020	12	Wehrlite
PA-A	1030	26	Sp-harzburgite
PA-A1	1196	22	Sp-lherzolite
PA-A2	1191	27	Wehrlite
PA-8	1260	24	Grt-harzburgite

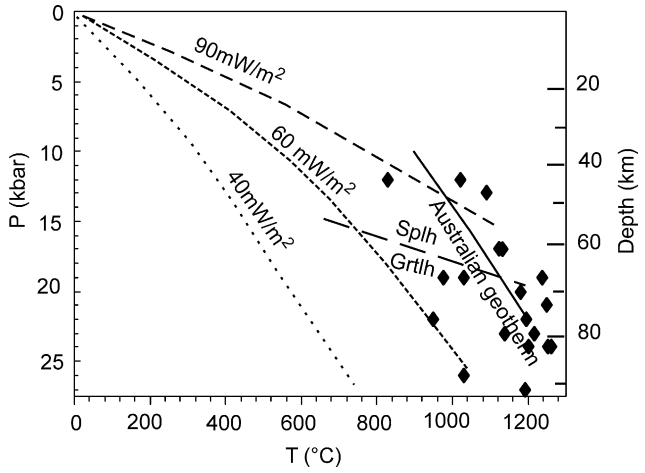

Fig. 8. *P–T* estimates for garnet- and spinel-bearing xenoliths from selected localities in Patagonia. Australian geotherm from O'Reilly and Griffin (1985).

and 23–24 kbar, whereas spinel lherzolites equilibrate at 1017 °C and 28 kbar.

High *P–T* conditions recorded in spinel lherzolites from Laguna Fría vary between 1230–1260 °C and 19–24 kbar. The spinel lherzolites from Laguna Fría contain characteristic pyroxene/Cr-spinel symplectites, which indicates that these rocks may have contained garnet as a stable Al-phase. In Gobernador Gregores, sp-lherzolite equilibration temperatures vary between 830 and 1090 °C and 12 and 13 kbar, whereas wehrlites equilibrate at 1080 °C and 11 kbar.

The calculated pressure and temperature of equilibration of the xenoliths in the mantle are both high and suggest a geothermal model gradient of approximately 13 °C/km for both Comallo (far NW of Patagonia) and Pali Aike (SE of Patagonia), which are separated by approximately 1500 km. This elevated geotherm (Fig. 8) is similar to that derived from xenoliths of southeast Australia (SEA, O'Reilly and Griffin, 1985) and estimations made for suboceanic thermal conditions. Such high geothermal gradients are unusual in comparison with expectations for below low heat flow continental cratons. A plausible explanation is the location of the Pliocene–Pleistocene Patagonian volcanism in a tectonically active backarc situation, as has been suggested by, among others, Stern et al. (1986).

8.5. Clinopyroxene composition

Variations of TiO_2, CaO, and Na_2O with Al_2O_3 contents in clinopyroxene (Fig. 9) reflect the influence of several processes. Garnet-bearing lherzolites (Pr-199, Pr-74) contain Al-rich clinopyroxene, which is poor in CaO and rich in Na_2O, reflecting the primitive bulk composition and high temperature of equilibration. The TiO_2 content is low because of preferential partitioning of Ti into garnet (O'Reilly and Griffin, 1995; Xu et al., 1998; van Achterbergh et al., 2003). Of the garnet-free lherzolites, only DUB-4G has a clinopyroxene composition comparable to that of the garnet-bearing rocks. It differs, however, because it has more CaO and TiO_2 in its clinopyroxene (at comparable Na_2O contents), which indicates a lower *T* of equilibration than the former, as well as clinopyroxene compositional equilibration in a garnet-free system. Two rocks with pyroxene-spinel symplectites (PA-Paike and Pr-1E) have clinopyroxene with Al_2O_3 contents almost as high as those in clinopyroxene of garnet-bearing rocks. In sample Pr-1E, the clinopyroxene is very poor in TiO_2, apparently because of its derivation from a garnet-bearing system. Clinopyroxene in samples PA-Paike and Pr-99 approaches the fractionation trend of clinopyroxene of garnet-free rocks in the TiO_2 versus Al_2O_3 projection. All other samples follow the liquid extraction trend toward low Al_2O_3 and TiO_2 contents, as defined by the end-members DUB-4G (fertile lherzolite) and Co-30 (depleted equigranular harzburgite). Clinopyroxene from the equigranular harzburgite TL-36 slightly deviates from the general trend, which indicates some metasomatic alteration.

A trend similar to that in TiO_2 versus Al_2O_3 contents is evident in the Na_2O versus Al_2O_3 abundances in clinopyroxene. The end members are Pr-199 (fertile garnet lherzolite) and TL-36 (depleted equigranular harzburgite). Again, the sample that deviates from the trend (Tr-2) has experienced metasomatic alteration.

The CaO versus Al_2O_3 contents in clinopyroxene exhibit two fractionation trends, one with garnet lherzolite Pr-199 and the other with spinel lherzolite DUB-4G as the fertile end member and harzburgite TL-36 as the depleted one. These two trends apparently reflect two different thermal regimes: a high-*T* defined by the garnet lherzolites and a low-*T* defined by DUB-4G.

9. Conclusions

Textural evidence shows that the lithospheric mantle beneath Patagonia is moderately to strongly tectonized and recrystallized on both local and regional scales, with an overall predominance of deformed textural types. It has experienced minor melt extractions in the garnet peridotite field and more extensive melt extractions in the spinel lherzolite field. A direct relationship between tectonism and partial melting processes is evidenced by the refractory xenoliths, which also exhibit the strongest deformation. No fertile lherzolites of primitive upper mantle chemical composition were encountered in Patagonia. All samples are strongly depleted in basaltic component. However, other than the samples from Prahuaniyeu, xenoliths from northern Patagonia are more depleted than are those of southern localities. Elemental depletion events were followed by intensive cryptic and modal metasomatism events, which affected the lithospheric mantle in this region.

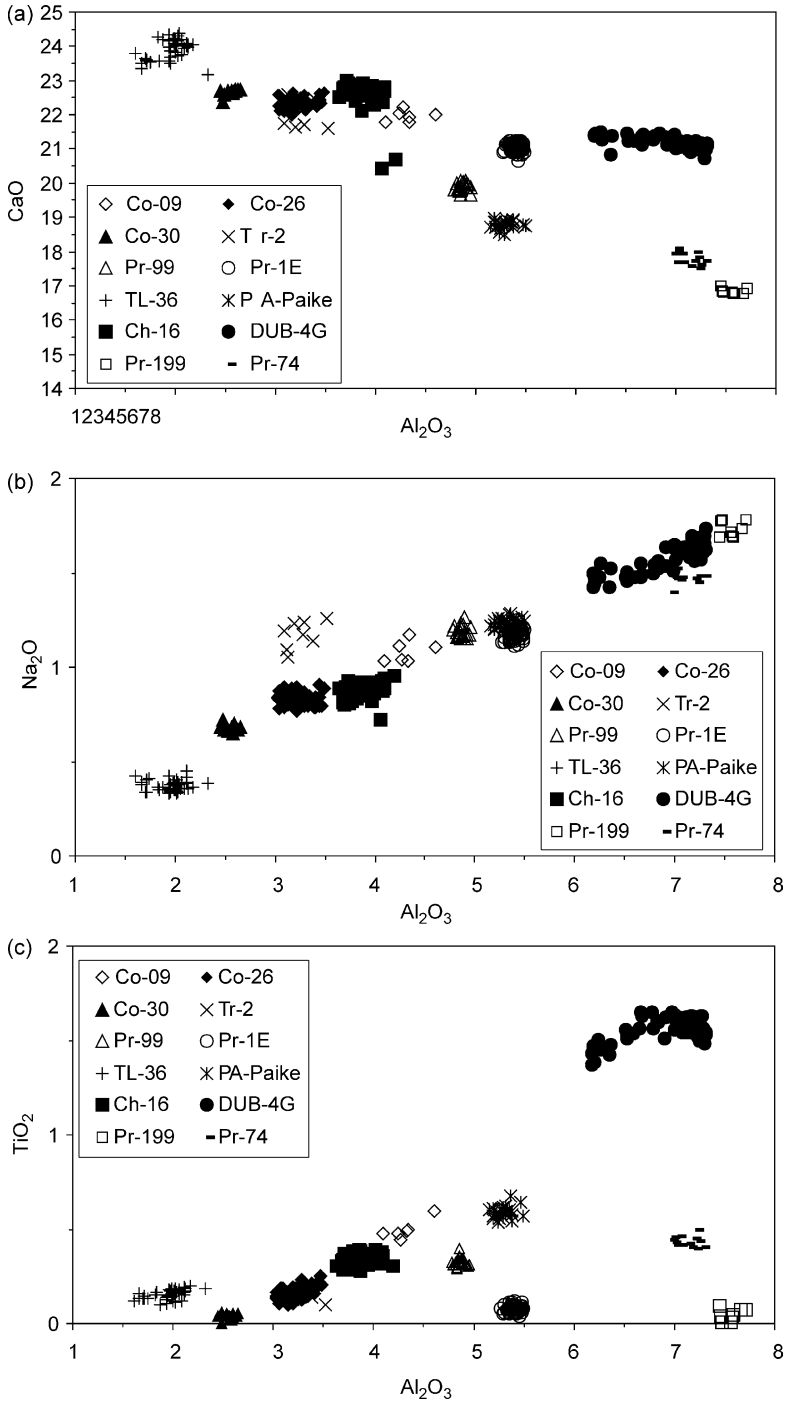

Fig. 9. Variation plots of contents of CaO, Na_2O, and TiO_2 versus Al_2O_3 in clinopyroxenes from Patagonian peridotites. (a) CaO versus Al_2O_3 abundances in two depletion trends: cpx of garnet lherzolite Pr 199 to harzburgite TL 36 (high-*T* trend) and from spinel lherzolite DUB 4G to TL 36 (low-*T* trend). Note the positions of cpx from symplectite-bearing peridotites Paike and Pr 1E. (b) Na_2O versus Al_2O_3 plot showing a smooth depletion trend from garnet lherzolite Pr 199 to sp harzburgite TL 36. (c) TiO_2 versus Al_2O_3 plot showing a depletion trend from sp lherzolite DUB 4G to sp harzburgite Co-30_A1. Clinopyroxenes of garnet- and symplectite-bearing peridotites deviate from this trend because Ti is preferentially partitioned into garnet. Deviations of clinopyroxenes in samples Pr 99-1 and TL 36 could reflect a memory effect on preexisting garnet and a metasomatic alteration, respectively.

Mineral equilibria suggest a strongly elevated geotherm underneath Patagonia, similar to the SEA and oceanic geotherms. This finding is not normal for a continental intraplate tectonic setting. Therefore, we suggest that the chemical and petrological features of the Patagonian upper mantle xenoliths may be related to rising mantle plume(s) in an extensional tectonic setting.

Acknowledgements

This work was supported by ANPCYT (Argentina) Grant PICT 97 Nr. 07-11791 to E.A.B. and by FWF (Austria), Grant P 11888-GEO to Th. N. and P 10670-GEO to G.K. The authors are grateful to Drs R. Fodor and Ch. Stern for valuable comments, which helped to improve the article.

Appendix A. Petrography and mineral chemistry

A.1. Comallo

Spinel harzburgites are dominant and show mosaic and tabular equigranular textures and transitional types.

Few olivine grains show narrow deformation lamellae, oriented parallel to the grain elongation. Some clinopyroxenes contain spinel exsolutions. Anhedral spinels show reddish-brown colors.

Websterites have transitional porphyroclastic to mosaic equigranular textures and some samples have mosaic equigranular textures. Spinel is located between silicate grains and in few cases as rounded inclusions. Sulfides are present as rounded inclusions and at silicate grain boundaries.

Interaction between host basalt and xenolith lead to the development of reaction rims around olivine and spinel grains located at the surface of the xenolith. Thin basaltic veins penetrate the xenoliths.

Metasomatism is evidenced by amphiboles (Fig. 2f, Table 2) enclosed by glass and newly formed clinopyroxene.

In spinel harzburgites, Fo contents in olivines average 92. Mean contents of Al_2O_3, Cr_2O_3 and FeO in orthopyroxenes (mean composition En_{91} Wo_1 Fs_8) are 2.30, 0.43 and 5.20 wt%, respectively. In clinopyroxenes, (mean composition En_{50} Wo_{47} Fs_3) the same oxides average contents are: 2.84, 1.00 and 2.20 wt%, respectively, and contents of CaO of 21.60, Na_2O 0.60 and TiO_2 0.47 wt%. The mg# and cr# in spinels are in the range 69 and 45, respectively. Number of studied samples: 4 (N = 4)

In websterites (N = 2), olivines have an average Fo content of 84 and contents of Al_2O_3, Cr_2O_3 and FeO in orthopyroxenes (mean composition En_{80} Wo_2 Fs_{18}) average 5.10, 0.05 and 11.40 wt%, respectively. The contents of the same oxides in clinopyroxenes (mean composition En_{44} Wo_{46} Fs_{10}) have the following average values: 6.40, 0.09 and 5.70 wt%, respectively. The contents of CaO, Na_2O and TiO_2 are 21.00–21.80, 0.54–0.77 and 0.55–0.70 wt%, respectively. Spinels have average mg# and cr# of 66 and 2, respectively.

Sulfides have mostly pentlandite composition.

A.2. Laguna Fría

The dominant rocks are spinel harzburgites and the dominant textures are porphyroclastic, transitional porphyroclastic to equigranular mosaic and equigranular mosaic.

In spinel harzburgites, olivine porphyroclasts show deformation lamellae. Orthopyroxenes carry clinopyroxene exsolutions that are bent. Spinels are anhedral and located at grain contacts. Some anhedral clinopyroxene grains carry orthopyroxene exsolutions restricted to the core of the crystals. In these xenoliths very good examples of orthopyroxene-clinopyroxene-spinel symplectites are present. Interstitial veins composed of olivine, spinel, orthopyroxene and light brown glass with bubbles are present.

In spinel harzburgites (N = 4), olivine displays a narrow compositional range: Fo 91. The contents of Al_2O_3, Cr_2O_3 and FeO in orthopyroxenes (mean composition En_{90} Wo_2 Fs_8) are 3.10, 0.52 and 5.20 wt%, respectively. Clinopyroxenes (mean composition: En_{54} Wo_{41} Fs_5) have Al_2O_3, Cr_2O_3, FeO and CaO contents of 3.50, 0.98, 1.92 and 21.80–23.10 wt%, respectively. The contents of Na_2O (0.40–0.71 wt%) and TiO_2 (0.59–0.61 wt%) are highly variable. For spinels the mg# and cr# are in the range 63–75 and 29–32, respectively.

In symplectites, orthopyroxene (mean composition En_{91} Wo_1 Fs_8) contents of Al_2O_3, Cr_2O_3 and FeO are 3.30, 0.69 and 5.40-. Clinopyroxene (mean composition En_{54} Wo_{41} Fs_5) Al_2O_3, Cr_2O_3, FeO and CaO contents of 3.50–3.90, 1.10–1.14, 2.88–3.16 and 19.77–20.30 wt%, respectively. The contents of Na_2O and TiO_2 are in the range 0.70–0.80 and 0.04–0.06 wt%.

Spinel has mg#: 71 and cr# 40.

A.3. Traful

Spinel harzburgites are the dominating rock type. Recrystallized rocks dominate followed by porphyroclastic ones and transitional porphyroclastic-equilibrated ones. Few composite samples with olivine websterite (clinopyroxene > orthopyroxene) vein cutting lherzolite have been recognized. Both rock types have mosaic equigranular texture. Spinels occur as anhedral spinel grains located between silicate contacts and small grains included in clinopyroxene. Olivines in the lherzolite show few deformation lamellae. Thin olivine veins rimmed by clinopyroxene cut the lherzolite. In xenoliths with mosaic equigranular and tabular textures, olivines have narrow deformation lamellae. Spinel is dark, anhedral, located at grain boundaries and in few cases as isolated inclusions in olivine. Serpentine-group minerals surround some spinels. Clinopyroxenes have spinel exsolutions. In spinel harzburgites with transitional porphyroclastic to mosaic equigranular textures, olivines show deformation lamellae (perpendicular to the crystal elongation). Spinels are anhedral and located at grain boundaries. Orthopyroxene have clinopyroxene exsolutions. Alteration veins composed

of serpentine-group minerals are present interstitially and in few cases, they crosscut the main silicate phases.

In harzburgites (N = 4), olivines display a narrow compositional range: Fo_{91}. The contents of Al_2O_3, Cr_2O_3 and FeO in orthopyroxenes (En_{91} Wo_1 Fs_8) are 2.42, 0.42 and 5.2 wt%, respectively. Clinopyroxenes (mean En_{51} Wo_{45} Fs_4) have contents of Al_2O_3, Cr_2O_3, FeO, CaO, Na_2O and TiO_2 of 2.1–3.2, 0.96, 2.30, 22.2, 0.46–0.90 and 0.30, respectively. For spinels the mg# and cr# are in the range 70–75 and 33–47, respectively. Spinels surrounded by serpentine show a rim that is rich in Cr_2O_3 (up to 35 wt%) compared to their core that is more aluminous (Al_2O_3 = 36.0 wt%, Cr_2O_3 = 18.0 wt%) and the associated serpentine is also rich in Cr_2O_3 (up to 4 wt%).

In symplectites, orthopyroxene (mean composition En_{91} Wo_1 Fs_8) contents of Al_2O_3, Cr_2O_3 and FeO are 1.90, 0.40 and 5.30. Clinopyroxene (mean composition En_{50} Wo_{47} Fs_3) Al_2O_3, Cr_2O_3, FeO and CaO contents of 2.40, 1.10, 1.90 and 23.20 wt%, respectively. The contents of Na_2O and TiO_2 are 0.60 and 0.03wt%. Spinel has mg# 70 and cr# 47.

In composite samples (N = 1), olivine websterite vein cutting spinel lherzolite, olivine has a very uniform composition, Fo_{92}. In orthopyroxene (mean En_{91} Wo_1 Fs_8) contents of Al_2O_3, Cr_2O_3 and FeO are 2.30, 0.50 and 5.40. In clinopyroxenes (mean En_{48} Wo_{49} Fs_3) contents of Al_2O_3, Cr_2O_3, FeO, CaO, Na_2O and TiO_2 are 2.20, 0.90, 1.82, 23.60, 0.35 and 0.15, respectively. Spinel has mg# 71 and cr# 40. In both rock types, the main mineral phases have the same composition, except spinel inclusions in olivine and clinopyroxene, which are Al_2O_3 rich (mg# 75, cr# 30).

A.4. Prahuaniyeu

Spinel lherzolites, harzburgites and websterites are the rock type present and have transitional protogranular to porphyroclastic and porphyroclastic textures where olivines display well-developed deformation lamellae. Some orthopyroxenes have clinopyroxene exsolutions and in some samples both spinel and clinopyroxene exsolutions are present. An interesting feature is the presence of orthopyroxene-clinopyroxene-spinel symplectites.

Garnet peridotites, garnet-spinel peridotites and garnet-bearing spinel clinopyroxenites have recently been documented in this area (Ntaflos et al., 2001, 2002). Garnet-bearing lherzolites and harzburgites are anhydrous and have equigranular textures, both mosaic and tabular. Garnet typically is surrounded by kelyphytic rims composed of a fine-grained intergrowth of orthopyroxene, clinopyroxene and spinel. In some cases, the garnet is completely replaced by this mineral association. Matrix clinopyroxenes develop spongy reaction rims. In garnet and spinel-bearing lherzolites, spinel is present as an interstitial phase. In those samples, garnets display very narrow kelyphytic rims (Fig. 2i) and occasionally garnet carry inclusions of olivines. Some spinels are surrounded by small sized olivine, orthopyroxene and clinopyroxene neoblasts, associated with a colorless to light brown glass. Thin glass veins are located interstitially and they have abundant bubbles.

Few composite samples consist of a websterite vein in a spinel harzburgite, both showing a mosaic equigranular texture. One of the samples is the only phlogopite-bearing sample encountered (Ntaflos et al., 2002), the hydrous phase is located in the websterite and surrounded by a fine-grained matrix composed of rutile, spinel, glass, olivine, sulfides and titanian augite. In this mosaic equigranular websterite, the orthopyroxenes carry spinel and clinopyroxene exsolutions, both of them restricted to the core of the host crystals.

Melt pockets constituted by glass, spinel, olivine and clinopyroxene are present in garnet-bearing harzburgites. Glass is present as veinlets located at the interface between matrix minerals and at the contact between spongy clinopyroxenes and both olivine and orthopyroxenes. Cu-Fe sulfides are present as rounded 'drop like' inclusions in the veins.

In porphyroclastic harzburgites (N = 3), Fo in olivine average 91. The contents of Al_2O_3, Cr_2O_3 and FeO in orthopyroxenes (mean composition En_{90} Wo_1 Fs_9) are 4.41, 0.46, 6.0wt%, respectively. Clinopyroxenes (mean En_{49} Wo_{47} Fs_4) also display a narrow range for the contents of Al_2O_3, Cr_2O_3, FeO and CaO: 5.41, 1.00, 2.55 and 21.0 wt%, respectively, while Na_2O and TiO_2 contents are 1.20 and 0.11 wt%, respectively. Spinel has mg# 74 and cr# 34.

In symplectites, orthopyroxene (mean composition En_{92} Wo_1 Fs_8) contents of Al_2O_3, Cr_2O_3 and FeO are 2.35, 0.50 and 5.15. In clinopyroxene, (mean composition En_{50} Wo_{47} Fs_3) Al_2O_3, Cr_2O_3, FeO and CaO contents are 2.30, 0.70, 1.85 and 23.50 wt%, respectively. The contents of Na_2O and TiO_2 are 0.45 and 0.01 wt%. Spinel has mg# 73 and cr# 32.

In garnet-spinel lherzolites (N = 3), olivine Fo contents average 90. The contents of Al_2O_3, Cr_2O_3 and FeO in orthopyroxenes (En_{88} Wo_3 Fs_9) are 4.9, 0.60, and 6.0 wt%, respectively. Clinopyroxenes (mean En_{52} Wo_{42} Fs_6) also display a narrow range in the contents of Al_2O_3, Cr_2O_3, FeO and CaO average: 6.20, 1.15, 3,10 and 18.5 wt%, respectively, and the contents of Na_2O (1.29wt%) and TiO_2 (0.36wt%) are constant. Garnets show a nearly constant composition, their mean end members are py: 73.1, alm: 12.8, gro: 8.7, and: 0, uv: 4.7 and sp: 0.7. Spinel's mean mg# and cr# are 78 and 21, respectively.

A.5. Gobernador Gregores

Spinel harzburgites and wehrlites are the dominating rock types. Coarse-grained anhydrous spinel harzburgites have protogranular textures. Olivines show kink-bands, orthopyroxenes have exsolution lamellae of clinopyroxene and green spinel. Clinopyroxenes are smaller than all other phases. Vermicular brown spinels occur as inclusions in orthopyroxene and olivine and at the triple points. No glass veins or melt pockets were found in this sample.

Coarse-grained amphibole-bearing wehrlites also show protogranular textures with typical 120° triple junctions.

Clinopyroxenes are green chromian diopsides showing spongy rims constituted by an intergrowth of pale-green clinopyroxene and brownish glass. Only few small grains of orthopyroxene in contact with clinopyroxene were found and matrix spinel is totally absent. Amphibole porphyroclasts (Table 2) commonly show reaction rims constituted by euhedral secondary olivine, clinopyroxene and spinel, calcite 'globules', brown silicate glass and vesicles (Fig. 2g). In some wehrlites, disseminated phlogopite (Table 2) is present instead of amphibole. Phlogopites, like amphiboles, have melt reaction rims or are penetrated by glass veinlets. At the triple junctions between olivine and clinopyroxene, melt-pockets up to 500 μm in diameter are present and they consist of glass, secondary calcite, relic amphibole and second-generation olivine, clinopyroxene and spinel.

In anhydrous spinel lherzolites with protogranular texture, large orthopyroxenes up to 1 cm in diameter have fine clinopyroxene exsolution lamellae restricted to their cores. The clinopyroxenes (5–1 mm across) exhibit 'spongy' rims composed of glass and secondary clinopyroxene. Melt pockets up to 8 mm in diameter contain glass, secondary calcite and secondary euhedral olivine, clinopyroxene and spinel and relics of primary olivine and reddish-brown spinel.

Anhydrous and melt pocket-free spinel lherzolites have transitional protogranular to equigranular textures. Large poikilitic clinopyroxenes and orthopyroxenes enclose smaller grains of olivine and brown spinel. The clinopyroxenes carry orthopyroxene and spinel exsolution lamellae and the orthopyroxenes have fine exsolution lamellae of clinopyroxene. Vermicular brown spinel occurs in the matrix as well as in both ortho- and clinopyroxene.

In anhydrous spinel lherzolites (N = 3), olivine Fo average contents are 91. The average contents of Al_2O_3, Cr_2O_3 and FeO in orthopyroxenes (mean En_{90} Wo_1 Fs_9) are 3.60, 0.57 and 5.50 wt%, respectively. In clinopyroxenes (mean En_{50} Wo_{45} Fs_5), the contents of the same oxides have are 5.35, 1.31 and 2.36 wt%, respectively, and the contents of CaO, Na_2O and TiO_2 are 20.65, 1.68 and 0.30 wt%, respectively. Spinel has mg# 56 and cr# 38.

In amphibole-bearing wehrlites (N = 2), average Fo in olivine is 89. The average contents of Al_2O_3, Cr_2O_3 and FeO in orthopyroxenes (mean En_{90} Wo_1 Fs_9) are 2.15, 0.55, 6.25 wt%, respectively. In clinopyroxenes (mean En_{51} Wo_{43} Fs_6), the same oxides average 3.80, 1.70 and 3.20 wt%, respectively, and CaO, Na_2O and TiO_2 20.5, 1.90 and 0.45 wt%, respectively. Spinel has mg# 43 and cr# 56.

A.6. Tres Lagos

Spinel harzburgites with porphyroclastic texture are dominant. Clinopyroxenes have bent exsolutions of orthopyroxene. Some orthopyroxenes have clinopyroxene exsolutions, which are restricted to the core of the grains. Clusters (symplectites) of orthopyroxene, clinopyroxene, and spinel are frequent in the spinel harzburgites. Anhedral spinel crystals are big (up to 1.2 mm) and olivines show deformation lamellae. Interstitial melt pockets consist of olivine, clinopyroxene and very small newly formed spinel. Light brown glass with bubbles is present at grain boundaries and in fractures. Few spinel lherzolites have been found and all have protogranular texture. Orthopyroxenes carry very fine clinopyroxene exsolution lamellae and clinopyroxene has coarse orthopyroxene exsolution lamellae. Greenish curvilinear spinel shows a reaction rim in contact with the surrounding phases.

Olivines in mosaic equigranular harzburgites (N = 3) average: Fo91. The mean contents of Al_2O_3, Cr_2O_3 and FeO in orthopyroxenes (mean En_{91} Wo_1 Fs_9) are 1.30, 0.35 and 5.80 wt%, respectively. Clinopyroxenes (mean En_{50} Wo_{47} Fs_3) average contents of Al_2O_3, Cr_2O_3, FeO, CaO, Na_2O and TiO_2: 1.42, 0.60, 2.10, 23.9, 0.41 and 0.08 wt%, respectively. Average mg# and cr# in spinels are 59 and 30, respectively.

In protogranular to porphyroclastic harzburgites (N = 4), Fo in olivine average 91. Orthopyroxenes (mean En_{91} Wo_1 Fs_8) have average contents of Al_2O_3, Cr_2O_3 and FeO of 1.65, 0.35 and 5.52 wt%, respectively, while in clinopyroxenes (mean En_{50} Wo_{46} Fs_4) the average contents of the same oxides are: 2.8, 0.98 and 2.02 wt%, respectively, and those of CaO, Na_2O and TiO_2 are 22.60, 0.85 and 0.25. Spinel has mg# 58 and cr# 28.

Orthopyroxene exsolutions in clinopyroxene have the following average contents of Al_2O_3, Cr_2O_3 and FeO: 2.35, 0.37, and 5.5 wt%, respectively, while the same oxides average contents in clinopyroxene exsolutions in orthopyroxene are 3.71, 1.13 and 2.22wt%, respectively, and those of CaO, Na_2O and TiO_2: 22.30, 0.89 and 0.39 wt%, respectively.

In lherzolites (N = 6) with protogranular to porphyroclastic textures, Fo in olivine average 90. In orthopyroxenes (En_{90} Wo_1 Fs_9), average contents of Al_2O_3, Cr_2O_3 and FeO are 3.80, 0.34 and 5.75 wt%, respectively, while in clinopyroxenes (En_{48} Wo_{48} Fs_4) the average content of the same oxides are 4.70, 0.79 and 2.35 wt%, respectively, and those of CaO, Na_2O and TiO_2 21.75, 1.22 and 0.37 wt%, respectively. Spinel has mg# 60 and cr# 26.

A.7. Pali Aike

Spinel harzburgites are the dominating rocks. They have protogranular to porphyroclastic transitional textures, some carry phlogopite crystals, clinopyroxenes have orthopyroxene exsolutions and vice versa. In both cases exsolution lamellae reach the surface of the host mineral. Olivine shows wide deformation lamellae and spinel is very scarce (below 2 vol%). Garnet harzburgites show porphyroclastic transitional to both tabular and equigranular mosaic textures. Olivine do not show deformation lamellae and both orthopyroxenes and clinopyroxenes are devoid of exsolutions. Small spinel grains are located interstitially.

In the spinel harzburgites (N = 7), Fo in olivine average 90. The average contents of Al_2O_3, Cr_2O_3 and FeO in orthopyroxene (En_{90} Wo_1 Fs_9) are 4.44, 0.51 and 6.05 wt%, respectively. Clinopyroxenes (mean En_{47} Wo_{50} Fs_3) have average contents of Al_2O_3, Cr_2O_3, FeO and CaO of 5.1, 0.93, 1.92 and 23.35 wt%, respectively and Na_2O and TiO_2 contents of 0.99 and 0.21 wt%, respectively. Spinel has #mg 74 and #cr 16.

Garnet harzburgites (N = 5) are rare and their average Fo content in olivine is 91. The contents of Al_2O_3, Cr_2O_3 and FeO in orthopyroxenes (En_{90} Wo_2 Fs_8) average 4.05, 0.57 and 5.95 wt%, respectively. In clinopyroxenes (mean En_{51} Wo_{44} Fs_5), average contents of Al_2O_3, Cr_2O_3, FeO and CaO are 4.95, 0.95 and 2.65 wt%, respectively, and for Na_2O and TiO_2 1.16 and 0.44 wt%. Garnets have a nearly constant composition, their mean end members are py: 74, alm: 12, gro: 4, and: 4, uv: 5 and sp: 1.

Few of the garnet harzburgites also carry spinels, whose mean mg# and cr# are 71 and 36, respectively.

References

Barbieri, M.A., 1998. Geochemical and petrologic characteristics of the mantle lithosphere in South America. Plinius 19, 125–129.

Barbieri, M.A., Zanetti, A., Mazzuchelli, M., Cingolani, C.A., Kempton, P.D., Vannucci, R., 1999. Garnet to spinel facies transition and related metasomatism in the mantle wedge of southern Patagonia (Pali Aike). Ofioliti 24 (1), 55–56.

Bjerg, E.A., Labudía, C.H., Cesaretti, N., 1991. Mineralogy, texture and stress measurements of mantle xenoliths from southern Argentina. European Journal of Mineralogy 3 (1), 31.

Bjerg, E.A., Labudía, C.H., Varela, E., Cesaretti, N., 1994. Fluid inclusions in olivine crystals from spinel lherzolites nodules, Somuncura Massif. Argentina. Revista de la Asociación Geológica Argentina 50 (1/4), 257–261.

Bjerg, E.A., Kurat, G., Ntaflos, Th., Labudía, C.H., 1999a. Patagonia mantle xenoliths: petrographic, geochemical and thermobarometric data, XIV Congreso Geológico Argentino, Actas II p. 88.

Bjerg, E.A., Kurat, G., Ntaflos, Th., Labudía, C.H., 1999b. A complex history of the Patagonian subcontinental upper mantle. Berichte der Deutschen Mineralogischen Gesellschaft. Beihefte zum European Journal of Mineralogy 11, 34.

Bjerg, E.A., Ntaflos, Th., Kurat, G., Frisicale, M.C., Ferracutti, G.R., Labudía, C.H., 2000. Caracterización petrográfica de xenolitos ultramáficos del norte de Patagonia in: Schalamuk, I., Brodtkorb, M., Etcheverry, R., (Eds.), Mineralogía y Metalogenia 60–66, La Plata, Argentina 2000.

Bjerg, E.A., Ntaflos, Th., Kurat, G., Labudía, C.H., Ferracutti, G.R., 2002. Mantle xenoliths from Patagonia: petrography, geochemistry and geothermobarometry, XV Congreso Geológico Argentino Actas III, 79–82, Calafate, Argentina 2002.

Blusztajn, J., Shimizu, N., 1994. The trace element variations in clinopyroxenes from spinel peridotite xenoliths from southwest Poland. Chemical Geology 111, 227–243.

Brey, G.P., Köhler, T., 1990. Geothermobarometry in four phase lherzolite II. New thermobarometers, and practical assessment of existing thermobarometers. Journal of Petrology 31, 1353–1378.

Caminos, R., 1999. Geología Argentina, Instituto de Geología y Minería, SEGEMAR, Anales No. 29, Buenos Aires 1999. 786 pp.

Dalton, J.A., Lane, S.J., 1996. Electron microprobe analysis of Ca in olivine close to grain boundaries; the problem of secondary X-ray fluorescence. American Mineralogist 81 (1/2), 194–201.

Dobosi, G., Bjerg, E.A., Kurat, G., Ntaflos, Th., 1999. The Upper Mantle beneath Patagonia: a LAM-ICP-MS study. Berichte der Deutschen Mineralogischen Gesellschaft. Beihefte zum European Journal of Mineralogy 11, 59.

Frey, F.A., Suen, C.J., Stockman, H.W., 1985. The Ronda high temperature peridotite: geochemistry and petrogenesis. Geochimica et Cosmochimica Acta 49, 2469–2491.

Gelós, E.M., Hayase, K., 1979. Estudiio de las inclusiones peridotíticas en un basalto de la región de Comallo y de otras localidades de las Provincias de Río Negro y Chubut, VI Congreso Geológico Argentino Actas II, 69–81, Buenos Aires, Argentina 1979.

Gelós, E.M., Labudía, C.H., 1981. Estudio de los basaltos con anfíboles y rocas asociadas de la Sierra de Queupu Niyeu, Provincia de Río Negro, República Argentina, VIII Congreso Geológico Argentino Actas IV, 921–933, Buenos Aires, Argentina 1981.

Horn, I., Hinton, R.W., Jackson, S.E., Longerich, H.P., 1997. Ultra-trace element analysis of NIST SRM 616 and 614 using laser ablation microprobe-inductively coupled plasma-mass spectrometry (LAM-ICP-MS): a comparison with secondary ion mass spectrometry (SIMS). Geostandards Newsletter 21, 191–203.

Jackson, S.E., Longerich, H.P., Dunning, G.R., Fryer, B.J., 1992. The application of laser ablation microprobe-inductively coupled plasma-mass spectrometry (LAM-ICP-MS) to in situ trace element determinations in minerals. Canadian Mineralogist 30, 1049–1064.

Jenner, G.A., Foley, S.F., Jackson, S.E., Green, T.H., Fryer, B.J., Longerich, H.P., 1994. Determination of partition coefficients for trace elements in high pressure–temperature experimental run products by laser ablation microprobe-inductively coupled plasma-mass spectrometry (LAM-ICP-MS). Geochimica et Cosmochimica Acta 58, 5099–5103.

Kilian, R., Stern, C.R., 2002. Constraints on the interaction between slab melts and the mantle wedge from adakitic glass in peridotite xenoliths. European Journal of Mineralogy 14, 25–36.

Kilian, R., Franzen, Ch., Koch, M., 1998a. The metasomatism of the mantle wedge below the southern Andes: constraints from laser ablation microprobe ICP-MS trace element analysis of clinopyroxenes, orthopyroxenes and fluid inclusions of mantle xenoliths. Terra Nostra 98 (5), 81.

Kilian, R., Stern, C.R., Olker, B., Altherr, R., 1998b. The P–T evolution within the lithosphere of southernmost South America since Jurassic recorded in mantle xenoliths of the Pali-Aike volcanic field. Terra Nostra 98 (5), 85.

Kilian, R., Stern, C.R., Koch, M., Franzen, C., 2002. Arc to back arc variations in the metasomatic history of the lithospheric mantle below southernmost South America, XV Congreso Geológico Argentino Actas III, 56–59, Calafate, Argentina 2002.

Köhler, T., Brey, G.P., 1990. Ca-exchange between olivine and clinopyroxene as a geothermobarometer calibrated from 2 to 60 kbar in primitive natural lherzolites. Geochimica et Cosmochimica Acta 54, 2375–2388.

Kruse, H., Spettel, B., 1979. A combined set of automatic and interactive programs for instrumental neutron activation analysis. Journal of Radioanalytical Chemistry 70, 427–434.

Labudía, C.H., Bjerg, E.A., Gregori, D.A., 1984. Nódulos de composición ultrabásica de las lavas alcalinas de la localidad de Praguaniyeu, provincia de Río Negro, IX Congreso Geológico Argentino Actas II, 547–553, Buenos Aires, Argentina 1984.

Labudía, C.H., Bjerg, E.A., Cesaretti, N., 1990. Nódulos lherzolíticos en basaltos alcalinos del Bajo de Lenzaniyeu, Provincia de Río Negro. Argentina. Revista de la Asociación Geológica Argentina 44 (1/4), 217–223.

Laurora, A., Rivalenti, G., Bottazzi, P., Barbieri, M.A., Cingolani, C.A., Vannucci, R., 1999. Carbonated peridotite xenoliths from the mantle wedge: the Patagonia case. Ofioliti 24 (1), 123–124.

Laurora, A., Mazzucchelli, M., Rivalenti, G., Vannucci, R., Zanetti, A., Barbieri, M.A., Cingolani, C.A., 2001. Metasomatism and melting in carbonated peridotite xenoliths from the mantle wedge: the Gobernador Gregores case (southern Patagonia). Journal of Petrology 42 (1), 69–87.

Mazzucchelli, M., Rivalenti, G., Vannucci, R., Zanetti, A., Ciuffi, S., Cingolani, C.A., 2002. The mantle lithosphere in northern Patagonia, XV Congreso Geológico Argentino Actas III, 85–88, Calafate, Argentina 2002.

McDonough, W.F., 1990. Constraints on the composition of the continental lithospheric mantle. Earth and Planetary Science Letters 101, 1–18.

Mercier, J.C.C., Nicolas, A., 1975. Textures and fabrics of upper-mantle peridotites as illustrated by xenoliths from basalts. Journal of Petrology 16 (2), 454–487.

Ntaflos, Th., Bjerg, E.A., Kurat, G., Labudía, C.H., 1998. Metasomatische Prozesse im Subkontinentalen Erdmantel unterhalb Süd-Patagoniens, Argentinien. Mitteilungen der Österreichischen Mineralogischen Gesellschaft Band 143, 357–358.

Ntaflos, Th., Bjerg, E.A., Kurat, G., Hinton, R., Labudía, C.H., Upton, B.G.J., 1999. Silicate and carbonatite melts in upper mantle xenoliths from southern Patagonia: evidence for multiple metasomatic events. Berichte der Deutschen Mineralogischen Gesellschaft, Beihefte zum European Journal of Mineralogy 11, 168.

Ntaflos, Th., Günther, M., Labudía, C.H., Bjerg, E.A., Kurat, G., Dingeldey, C., 2000. Isotopic and geochemical evolution of the Cenozoic basalts from Rio Negro, 31st International Geological Congress, Abstracts Volume, Río de Janeiro, Brazil 2000.

Ntaflos, Th., Bjerg, E.A., Labudía, C.H., Thöni, M., Frisicale, C., Günther, M., 2001. Garnet-bearing xenoliths: evidence of plume activity in northern Patagonia, 11 Annual V.M. Goldschmidt Conference Abstracts, Hot Springs, Virginia, USA 2001.

Ntaflos, Th., Bjerg, E.A., Labudía, C.H., 2002. High temperature, low pressure garnet-peridotites from Praguaniyeu: evidence for plume activity in northern Patagonia, XV Congreso Geológico Argentino Actas III, 53–55, Calafate, Argentina 2002.

O'Reilly, S.Y., Griffin, W.L., 1985. A xenolith-derived geotherm for southeastern Australia and its geophysical implications. Tectonophysics 111, 41–63.

O'Reilly, S.Y., Griffin, W.L., 1995. Trace-element partitioning between garnet and clinopyroxene in mantle-derived pyroxenites and eclogites: *P-T-X* controls. Chemical Geology 121 (1/4), 105–130.

Ramos, V.A., 1999. Plate tectonic setting of the Andean Cordillera. Episodes 22 (3), 183–190.

Rivalenti, G., Vannucci, R., Zanetti, A., Mazzucchelli, M., Laurora, A., Ciuffi, S., Cingolani, C.A., 2002. Composition and processes of the South America mantle lithosphere in Patagonia, XV Congreso Geológico Argentino Actas III, 89–94, Calafate, Argentina 2002.

Skewes, M.A., Stern, C.S., 1979. Petrology and geochemistry of Alkali Basalts and ultramafic inclusions from the Pali Aike volcanic field in southern Chile and the origin of Patagonian Plateau Lavas. Journal of Volcanology and Geothermal Research 6, 3–25.

Stern, C.R., 1989. Sr^{87}/Sr^{86} of mantle xenoliths bearing Plio-Quaternary alkali basalts of the Patagonian Plateau lavas of southernmost South America. Revista de la Asociación Geológica Argentina 44 (1/4), 402–407.

Stern, C.R., Kilian, R., 1996. Role of the subducted slab, mantle wedge and continental crust in the generation of adakites from the Andean Austral Volcanic Zone. Contributions to Mineralogy and Petrology 123, 263–281.

Stern, C.R., Futa, K., Saul, S., Skewes, M.A., 1986. Nature and evolution of the subcontinental mantle lithosphere below southern South America and implications for Andean magma series. Revista Geológica de Chile 27, 41–53.

Stern, C.R., Frey, F.A., Futa, K., Zartman, R.E., Peng, Z., Kyser, T.K., 1990. Trace-element and Sr, Nd, Pb, and O isotopic composition of Pliocene and Quaternary alkali basalts of the Patagonian Plateau lavas of southernmost South America. Contributions to Mineralogy and Petrology 104, 294–308.

Stern, C.R., Kilian, R., Olker, B., Hauri, E.H., Kyser, T.K., 1999. Evidence from mantle xenoliths for relatively thin-100 km continental lithosphere below the Phanerozoic crust of southernmost South America. Lithos 48, 217–235.

Sun, S., McDonough, W.F., 1989. Chemical and isotopic systematics of oceanic basalts: implications for mantle composition and processes, in: Saunders, A.D., Norry, M.J. (Eds.), Magmatism in the Ocean Basins Geological Society of London Special Publication 42, pp. 313–345.

van Achterbergh, E., Griffin, W.L., Shee, S.R., Wyatt, B.A., Sharma, A.L., 2003. Natural trace element distribution coefficients for garnet, clino- and orthopyroxene: variations with temperature and pressure, 7th International Kimberlite Conference, Cape Town, South Africa. Abstract Volume 2003.

Vannucci, R., Zanetti, A., Kempton, P.D., Ciuffi, S., Mazzucchelli, M., Cingolani, C.A., 2002. The chemical history of young lithospheric mantle in a back-arc region: the spinel $\pm$ garnet peridotite xenoliths from Pali Aike (South Patagonia), XV Congreso Geológico Argentino Actas III, 71–74, Calafate, Argentina 2002.

Varela, M.E., Bjerg, E.A., Labudía, C.H., 1995. Fluid inclusion evolution in upper mantle xenoliths from Patagonia, Argentina. XIII ECROFI Symposium, Sitges (Spain). Boletín de la Sociedad Española de Mineralogía 18 (1), 256–257.

Varela, M.E., Bjerg, E.A., Clocchiatti, R., Labudía, C.H., Kurat, G., 1997. Fluid inclusions in upper mantle xenoliths from northern Patagonia, Argentina: evidence for an upper mantle diapir. Mineralogy and Petrology 60, 145–164.

Villar, L.M., 1975. Las fajas y otras manifestaciones ultrabásicas de la República Argentina y su significado metalogenético, II Congreso Geológico Iberoamericano de Geología Económica Actas III, 135–156, Buenos Aires, Argentina 1975.

Walter, M.J., Presnall, D.C., 1994. Melting behaviour of simplified lherzolite in the subsystem $CaO–MgO–Al_2O_3–SiO_2–Na_2O$ from 7 to 35 kbar. Journal of Petrology 35, 329–359.

Xu, X., O'Reilly, S.Y., Griffin, W.L., Zhou, X., Huang, X., 1998. The nature of the Cenozoic lithosphere at Nushan, eastern China, in: Flower, M., Chung, S.L., Lo, C.H., Lee, T.Y. (Eds.), Mantle Dynamics and Plate Interactions in East Asia American Geophysical Union, Geodynamics Series, vol. 27, pp. 167–196.